Title

Structure of a D2 dopamine receptor–G-protein complex in a lipid membrane

Journal

Nature, 584(7819)

ISSN

0028-0836

Authors

Yin, Jie
Chen, Kuang-Yui M
Clark, Mary J
et al.

Publication Date

2020-08-06

DOI

10.1038/s41586-020-2379-5

Peer reviewed

Published in final edited form as:

Nature. 2020 August ; 584(7819): 125–129. doi:10.1038/s41586-020-2379-5.

Structure of a D_2 dopamine receptor-G protein complex in a lipid membrane

Jie Yin[1], **Kuang-Yui M. Chen**[2], **Mary J. Clark**[3], **Mahdi Hijazi**[2], **Punita Kumari**[1], **Xiao-chen Bai**[1], **Roger K. Sunahara**[3,*], **Patrick Barth**[2,*], **Daniel M. Rosenbaum**[1,*]

[1]Department of Biophysics, The University of Texas Southwestern Medical Center, Dallas, Texas 75390, USA [2]Institute of Bioengineering, Swiss Federal Institute of Technology (EPFL), Lausanne, Switzerland [3]Department of Pharmacology, University of California San Diego School of Medicine, La Jolla, California 92093, USA

Abstract

The D_2 dopamine receptor (DRD2) is a therapeutic target for Parkinson's disease[1] and antipsychotic drugs[2]. DRD2 is activated by the endogenous neurotransmitter dopamine and synthetic agonist drugs such as bromocriptine[3], leading to stimulation of G_i and inhibition of adenylyl cyclase. We used cryo-electron microscopy to elucidate the structure of an agonist-bound activated DRD2-G_i complex reconstituted into a phospholipid membrane. The extracellular ligand binding site of DRD2 is remodeled in response to agonist binding, with conformational changes in extracellular loop 2 (ECL2), transmembrane domain 5 (TM5), TM6, and TM7 propagating to opening of the intracellular G_i binding site. The DRD2-G_i structure represents the first experimental model of a GPCR-G protein complex embedded in a phospholipid bilayer, which serves as a benchmark to validate the interactions seen in previous detergent-bound structures. The structure also reveals interactions that are unique to the membrane-embedded complex, including helix 8 burial in the inner leaflet, ordered lysine and arginine sidechains in the membrane interfacial regions, and lipid anchoring of the G protein in the membrane. Our model of the activated DRD2 will help inform the design of subtype-selective DRD2 ligands for multiple human CNS disorders.

[*]corresponding authors: Daniel Rosenbaum, Department of Biophysics, The University of Texas Southwestern Medical Center, Dallas, Texas 75390, USA, Phone: (214)648-4151, dan.rosenbaum@utsouthwestern.edu, Patrick Barth, Institute of Bioengineering, Swiss Federal Institute of Technology (EPFL), Lausanne, Switzerland, patrick.barth@epfl.ch, Roger Sunahara, Department of Pharmacology, University of California at San Diego, La Jolla, California, rsunahara@ucsd.edu.

Author Contributions

J.Y. expressed and purified the DRD2-G_i complex; collected cryo-EM data; and carried out cryo-EM reconstructions. K.M.C. carried out computational design calculations on DRD2 mutants and performed in vitro experimental characterization of the designed DRD2 constructs. M.J.C. collected functional data on DRD2 constructs. M.H. carried out molecular dynamics simulations of DRD2. P.K. assisted with DRD2 purification and testing of mutants. X.B. supervised cryo-EM data collection and analysis. R.K.S. supervised collection of functional data on DRD2 constructs and helped write the manuscript. P.B. developed the strategy for computational design of a stabilized DRD2 active state construct and supervised computational design calculations. D.M.R supervised the overall project, assisted with cryo-EM data analysis, and wrote the manuscript.

Author Information

Correspondence and requests for materials should be sent to D.M.R. at dan.rosenbaum@utsouthwestern.edu, P.B at patrick.barth@epfl.ch., or R.K.S. at rsunahara@ucsd.edu.

Keywords

dopamine; dopamine receptor; GPCR; G protein; cryo-EM; Parkinson's disease

Dopamine signaling through dopamine receptors

Dopamine is an essential neurotransmitter that regulates multiple physiological and cognitive functions including movement, reward, and emotion. DRD2 signaling is impaired in Parkinson's disease, in which dopaminergic neurons are damaged and a deficit of dopamine leads to a combination of movement and psychiatric pathologies[4]. Parkinson's disease is currently treated by dopamine replacement therapies, either with the prodrug L-dopa or analogs that can act directly on DRD2. Agonists such as bromocriptine have also been effectively used against pituitary adenomas[5]. Conversely, inhibitors of DRD2 are used in schizophrenia and psychosis, in order to reduce elevated dopaminergic signaling[6].

The dopamine family of G protein-coupled receptors (GPCRs) contains 5 subtypes, D_1-D_5, which have partially overlapping functions and pharmacology[1]. The receptors D_1 and D_5 couple to the stimulatory G protein G_s, while $D_2/D_3/D_4$ couple mainly to $G_{i/o}$ (inhibitory toward cAMP). At a sequence level, D_1 and D_5 share high overall homology (58% identity, 79% similarity) and $D_2/D_3/D_4$ are likewise closely related (40–57% identity, 60–70% similarity)[7]. Despite the division between these receptor families, key residues that bind dopamine are highly conserved in all 5 receptors. For therapeutic ligands that target DRD2 in Parkinson's and schizophrenia, subtype and/or family selectivity has been pursued to maximize efficacy and minimize off-target effects[8].

Structural biology of the dopamine receptors and G protein complexes

The structure of DRD2 bound to the inverse agonist risperidone was previously determined using an engineered T4L fusion protein[9], elucidating the overall inactive conformation and the molecular basis for inhibitor binding. The structure also demonstrated how risperidone can bind to D2-family receptors (DRD2, DRD3, DRD4) with selectivity over the D1 family (DRD1 and DRD5), based on interactions with an extended binding pocket including the extracellular loops. The structures of inhibitor-bound inactive conformations of other dopamine receptors DRD3[10] and DRD4[11] have also been reported using engineered fusion proteins. To date, no structure of an activated dopamine receptor has been reported. In contrast, activated GPCR-G protein complexes have recently been structurally characterized by cryo-electron microscopy (cryo-EM) for μ opioid[12] and CB1 cannabinoid[13] receptors, among others. Common to all these studies is the use of detergent micelles to solubilize the receptor and allow co-purification with G protein as single particles, with the caveat that the complexes lack the phospholipid bilayer environment important in receptor regulation and G protein recruitment. Indeed, early purification of endogenous DRD2 from bovine pituitary showed that the detergent-solubilized receptor has compromised ligand binding properties[14]. Previous work established the use of reconstituted HDL particles[15,16] (also known as lipid nanodiscs[17]) as effective host membranes for biochemical and biophysical studies of GPCRs and their G protein complexes. These systems have been exploited for cryo-EM structure

determination of other membrane proteins such as ion channels[18], as well as for the full-length mGlu5 Family C GPCR[19] and the M_2 acetylcholine receptor-arrestin complex[20], however no such structures have been reported for GPCR-G protein complexes. In this work, we report the first structure of an agonist-bound D2 dopamine receptor bound to G_i in an HDL/nanodisc system containing native lipids.

DRD2 construct design and cryo-EM structure determination

To obtain a human DRD2 construct optimized for active-state structure characterization, we computationally designed mutations that would shift the ligand-free receptor towards the active state by lowering the free energy of a modeled active conformation and raising the free energy of the inactive conformation (Methods, Extended Data Figs. 1a–e). The resulting construct bears 5 mutations relative to the wild-type human DRD2, none of which are at the orthosteric pocket. Because the native hDRD2 has a 120-residue intracellular loop 3 (ICL3) that could hinder purification and structural characterization, we *de novo* designed a 7-residue ICL3 compatible with G_i binding (Methods, Extended Data Fig. 1f). We also incorporated an N-terminal T4L (nT4L) domain, as previously described for β_2AR[21], producing the final construct hDRD2^{EM}. Inclusion of the nT4L and truncation/modification of ICL3 did not alter dopamine binding (Extended Data Fig. 2a) or agonist-mediated (dopamine or bromocriptine) stimulation of G_i (Extended Data Fig. 2b). As would be predicted based on its altered allosteric equilibrium, our designed receptor hDRD2^{EM} has elevated constitutive activity, higher affinity for agonists such as dopamine and bromocriptine, and lower affinity for the inverse agonist spiperone (Extended Data Fig. 3a–c). In addition, the designed mutations confer enhanced thermostability compared to the wild-type hDRD2 (Extended Data Fig. 3e, f).

After screening commercially available agonists, we found that addition of the high-affinity agonist bromocriptine[3] permitted solubilization and purification of hDRD2^{EM}. Importantly, bromocriptine displays full agonism towards hDRD2^{EM}, and a lower EC_{50} relative to dopamine consistent with its higher affinity[22] (Extended Data Fig. 3c). We could efficiently co-purify a stable complex between hDRD2^{EM} and G_i (Extended Data Fig. 4a, b), however constructs without the 5 active-state mutations or with intact full-length ICL3 displayed poor biochemical behavior upon detergent solubilization (Extended Data Fig. 4c). The purified hDRD2^{EM}-G_i complex was further stabilized by addition of scFv16[12,13] that binds to the Gα and Gβ subunits away from the receptor interface, which also does not perturb ligand binding to wild-type hDRD2 (Extended Data Fig. 2b, c). This sample was reconstituted from detergent into nanodiscs containing a lipid mixture of palmitoyl-oleoyl-phosphatidylcholine (POPC), palmitoyl-oleoyl-phosphatidylglycerol (POPG), and cholesterol (3:2:1 molar ratio) along with the MSP1D1 scaffold peptide[23]. The final reconstituted complex was frozen in vitreous ice for single-particle cryo-EM analysis. We collected 9760 images on a Titan Krios microscope and obtained a reconstruction of the reconstituted hDRD2^{EM}-G_i complex at 3.7 Å resolution. Representative class averages and data analysis flowchart are included in Extended Data Figure 5 & 6, and associated statistics are included in Extended Data Table 1. The cryo-EM maps show strong density for the TM domains of DRD2 including sidechains (Extended Data Fig. 6d), without large variation in local resolution (Extended Data Fig. 5c).

Global structure of the DRD2-Gi complex reconstituted into a phospholipid bilayer

The overall reconstruction of DRD2-G_i in phospholipid bilayers is shown in Figure 1a, with the resulting model for receptor, ligand and G_i heterotrimer in Figure 1b. The structure is similar in global arrangement to previous GPCR-G_i complexes, with a notable difference in the asymmetric position of the receptor in the rHDL/nanodisc particle (Fig. 1a). From the receptor on one side to the G protein-bilayer contacts on the other, the protein complex fits tightly into the rHDL/nanodisc. Previous biochemical studies demonstrated that monomeric β_2 adrenergic receptor (β_2AR) embedded in rHDL fully retains its pharmacological properties, couples to G_s and stimulates nucleotide exchange[15]. Our reconstruction provides a structural basis for such activity, as the G protein footprint is accommodated within the ~80 Å inner diameter of the rHDL particle. Compared to the CB1-G_i complex in micelles[13], DRD2 in our reconstruction is tilted 10 degrees relative to the membrane-proximal surface of G_i (i.e. Gα's N-terminal helix αN) which positions the receptor's helix 8 in the membrane interfacial region (a larger translation of receptor relative to G_i is present in comparison with μOR-G_i[12]) (Fig. 1c). These differences reflect the fact that the phospholipid membrane places a physical constraint on the elements of the receptor and G protein that can come into contact. The structure of $hDRD2^{EM}$ in the complex is in close agreement with our computationally designed active-state conformation (Fig. 1d, Cα rmsd 2.1 Å overall and 1 Å for the TM helices).

Agonist binding to DRD2

Bromocriptine is an ergot alkaloid that acts as a full agonist at DRD2. In studies using subtype-selective radioligand antagonists as probes, bromocriptine displayed 2–5 nM affinity towards mammalian DRD2 and roughly 100-fold selectivity over DRD1, DRD4, and DRD5 (with little discrimination against DRD3)[22]. The residues interacting directly with bromocriptine in the active-state structure are shown in Figure 2a, and the cryo-EM density surrounding the ligand is displayed in Figure 2b. The ergoline core of bromocriptine is sandwiched between TM3 and TM6, and contains atoms analogous to the dopamine skeleton (Fig. 2c). As in other catecholamine receptors[24], the binding pocket is flanked on one side by an aspartate on TM3 ($Asp114^{3.32}$) forming a salt bridge with the agonist amino group, and on the other side by a cluster of serines on TM5 ($Ser193^{5.42}$, $Ser194^{5.43}$, $Ser197^{5.47}$), which are important for dopamine binding and activation[25,26]. The dopamine-like core of bromocriptine packs against $Phe389^{6.51}$ and $Phe390^{6.52}$ on TM6, in good agreement with biochemical precedent[27]. The bicyclic tripeptide group of the ligand extends toward the extracellular surface, primarily contacting residues on TM7 and extracellular loop 2 (ECL2) including $Ile184^{ECL2}$ previously characterized as lining the ligand binding pocket[28]. The ECL2 sequences of DRD1 and DRD5 are completely divergent from DRD2, which helps to explain the agonist's selectivity against those receptors. Bromocriptine and related ergopeptines are unique among DRD2 agonists in displaying single-site high affinity binding that is independent of G protein coupling (i.e. with or without the presence of GTP)[22,29,30]. The bivalent nature of bromocriptine's interaction with DRD2 (Fig. 2a) prevents closure of the extracellular lid of the receptor, which was shown to be critical for

high-affinity agonist binding in β_2AR[31]. The extensive interface of bromocriptine with DRD2 may allow for slow dissociation and resulting low-nM affinity even when the receptor is in an inactive conformation. Bromocriptine's binding overlaps with the interaction of risperidone (Fig. 2c), however the inverse agonist extends into a deeper subpocket in the inactive conformation[9], which contracts in the active conformation (Extended Data Fig. 7).

Propagation of conformational changes from dopamine to G_i

Comparison of the activated receptor in the G_i complex with the inverse agonist-bound structure shows how changes at the dopamine binding pocket are translated through the receptor to facilitate nucleotide exchange on the bound G_i. Bromocriptine binding at the orthosteric pocket occurs with rotation of the upper half of TM5 toward TM4 (Fig. 3a), concomitant with rigid body shifts of the extracellular halves of TM6 and TM7 inward toward the ligand and movement of ECL2 over the pocket. Residues Phe189$^{5.38}$ and Ile184^{ECL2} play an important role in this conformational change, since the swivel of the Phe189$^{5.38}$ phenyl group makes room for a downward shift of the Ile184^{ECL2} sidechain. Recent studies have implicated these two residues' movement in DRD2 activation, as well as in variable interaction with arrestin-biased agonists[32,33]. Repacking of sidechains in these upper TM segments (Fig. 3a) results in a downward shift in Trp386$^{6.48}$, formation of an active PIF transmission switch (Fig. 3b), and outward movement of the bottom half of TM6 by 11.9 Å (measured between E368$^{6.30}$ C_α's), all hallmarks of GPCR activation[34]. The designed V378$^{6.40}$Y mutation at the apex of the G_i binding site helps to stabilize the TM6-out active conformation by packing against Tyr426$^{7.53}$ and Arg132$^{3.50}$ of the DRY motif (Extended Data Fig. 8), interactions that are not present in the inactive conformation.

The interaction between DRD2 and G_i in rHDL/nanodiscs buries 2,856 Å^2 (Fig. 3c). Like the CB1-G_i[13], μOR-G_i[12], or β_2AR-G_s[35], the most extensive contacts occur between TM5, TM6, TM7, and ICL2 of the receptor and the α5 helix of the G protein. As in the μOR-G_i complex (but not in CB1-G_i), DRD2's ICL2 makes multiple contacts with the $G\alpha_i$ αN helix that extends along the membrane surface. Similar to the β_2AR-G_s crystal structure in monoolein bilayers, DRD2 also contacts the Gβ subunit through residues on ICL1 and ICL2 (Fig. 3c). Engagement by DRD2 causes a 5 Å translation and 60° rotation of the α5 helix relative to the GDP-bound free G[36], similar to other complexes, resulting in movement of the TCAT motif on the β6-α5 loop away from the nucleotide and movement of the P-loop into space sterically overlapping with GDP binding (Fig. 3d). During 3D classification of our cryo-EM dataset (Extended Data Fig. 5), we also observed weaker density corresponding to the alpha-helical (AH) domain of $G\alpha_i$, and after focused refinement on the G protein (Extended Data Fig. 6b), we could dock the AH domain into density as a rigid body (Fig. 3d, Extended Data Fig. 9a). The AH domain in DRD2-G_i is positioned similarly to its site in the rhodopsin-G_i[37] (Extended Data Fig. 9b–d), implying that these two structures may represent a low-energy conformation within nucleotide-free GPCR-G_i complexes despite the AH domain's well-characterized flexibility[21,35].

Interactions specific to the DRD2-G_i complex in the rHDL/nanodisc

G protein subunits are specifically acylated, which is essential for their trafficking to the plasma membrane and the formation of functional heterotrimers. $G\alpha_i$ is first myristoylated at the N-terminal Gly2 residue[38] and then reversibly palmitoylated at the following Cys3 position[39], whereas $G\gamma$ is geranylgeranylated at the C-terminal CAAX motif which is important for membrane association of $G\beta\gamma$ and $G\alpha$ recruitment[40]. Disruption of the lipid modifications on $G\alpha_i$ by mutagenesis impairs agonist-dependent inhibition of adenylyl cyclase[41]. In our reconstruction of DRD2-G_i in rHDL/nanodiscs, the αN helix runs along the outer surface of the bilayer (Fig. 4), where positively charged residues Lys10, Lys17, and Arg24 project up to interact with the polar membrane headgroups. Weak density could be observed at the ends of the $G\alpha_i$ and $G\gamma$ subunits by cryo-EM, however we could not accurately model the acylated residues or lipid modifications themselves (presumably due to disorder). What has not been apparent in structures of GPCR-G protein complexes reported to date is the lipid association of Gβ, other than its tight association with the acylated $G\gamma$. In the reconstituted DRD2-G_i complex, we observe density for basic residues Arg42, Arg46 and Arg52 of Gβ, which interact with the polar lipid headgroups (Fig. 4). Likewise, Arg62 and Lys64 on the C-terminal portion of $G\gamma$ are also well-ordered and interact with the lipid headgroups of the phospholipid bilayer. These collective polar interactions between the G_i heterotrimer and the lipid headgroups, together with $G\alpha_i$ and $G\gamma$ acylation, highlight the critical role of the phospholipid bilayer in receptor-G protein coupling.

The amphipathic helix 8 in Class A GPCRs often contains a cysteine residue that can be reversibly palmitoylated, represented by Cys443 in DRD2. Lipidation of the receptor is important for partitioning of helix 8 into the membrane[42], and in cases such as β_2AR depalmitoylation is regulated by agonist stimulation[43]. We were unable to model the palmitate moiety in DRD2, most likely because it is disordered within the membrane (although it is possible that some fraction of the palmitate was hydrolyzed during purification). Strikingly, helix 8 in the activated DRD2-G_i complex is entirely embedded within the phospholipid membrane interfacial region (Fig. 4), in agreement with model studies of rhodopsin helix 8 peptides in membranes using fluorescence quenching by brominated lipids[44]. The attitude of helix 8 within the membrane positions residues Phe429$^{7.56}$, Asn430, and Glu432 at the TM7-helix 8 junction to participate in the interface with the C-terminus of $G\alpha_i$'s α5 helix. The degree to which helix 8 is embedded in the bilayer again highlights the importance of the lipid membrane in receptor structure and function.

DRD2, like many GPCRs, has an abundance of positively charged basic residues on the cytoplasmic side of the membrane, in accordance with the 'positive-inside rule' for α-helical membrane proteins[45]. We observe strong density for a number of these arginine and lysine sidechains in the inner leaflet interfacial region (e.g. Arg61$^{1.59}$, Arg151$^{4.41}$, Arg217$^{5.66}$, Lys370$^{6.32}$, Lys439), which may reflect energetically favorable interactions with lipid headgroups and conformational restriction previously characterized in MD simulations of basic residues in model TM helices[46]. These basic residues create a positively charged 'ring' at the membrane surface that is complementary to electrostatically negative surfaces on the G_i heterotrimer (Extended Data Fig. 10).

The distinctive features of this complex may be specific to the DRD2-G_i interaction, but more likely reflect general features of GPCR-G protein complexes in membranes. As we elucidate additional structures of receptors in a more native-like phospholipid bilayer environment (rHDL/nanodiscs), more light will be shed on how the membrane contributes to the molecular mechanism of G protein coupling and specificity.

Methods

Computational modeling of DRD2 active and inactive states

The inactive and active state structures of DRD2 WT were modeled from the close homolog inactive state structure of DRD3 (3PBL) and the more distant homolog active state structure of β_2AR, respectively, using the software iPHoLD[47]. Low energy representative models of the DRD2 WT were selected for design calculations, as previously described.

Computational design of residue microswitches

The TM region of DRD2 was subjected to complete multi-state design using a fitness function selecting residue microswitches stabilizing the active state structure while decreasing the allosteric coupling between the extracellular ligand binding site and the inactive state conformation of the intracellular G protein binding site. Conformational stability was assessed using an all-atom energy function developed for membrane protein modeling and design. Allosteric couplings were approximated by the correlated dynamic fluctuations between allosteric residues using normal mode calculations[48].

Computational *de novo* design of minimal intracellular loop 3

The kinematic loop design protocol of Rosetta was used to *de novo* design short loop structures and sequences connecting the cytoplasmic ends of TM5 and TM6. Loop structures and sequences were selected to maximize stability and optimize conformation for $G\alpha_i$ binding. Loop lengths of three to nine amino acids were tested and the predicted models were clustered, selected by energy and structurally analyzed for distortions of the TM5/6 helical tips. Several designed loops of five to seven residues adopted stable helical structures enabling proper $G\alpha_i$ binding. Selected sequences from these loops with further refined with RosettaMembrane on active state DRD2 models onto which a peptide corresponding to the $G\alpha_i$ C-terminal $\alpha5$ helix was docked. The final selected 7 residue long designed ICL3 was predicted to retain native receptor-G protein TM contacts while stabilizing the DRD2 active conformation.

Mutagenesis and expression of receptors in HEK293 cells for stability assays

Quickchange PCR mutagenesis (Stratagene) was performed on the HA-tagged human DRD2 gene in the pcDNA3.1(+) vector. Sequenced mutant plasmids were transiently transfected using lipofectamine (Invitrogen) into HEK293T cells for DRD2 as previously described[48]. Briefly, 5×10^6 cells were plated on 10 cm tissue culture plates and grown overnight. This was followed by transfection with Lipofectamine 2000 (Invitrogen) and 2 μg of DNA per plate. After 24 hours, the cells were washed with PBS and grown in standard growth medium (DMEM supplemented with L-glutamine (2 mM), penicillin (100 mg/mL), streptomycin (100 mg/mL), and fetal bovine serum (10%)) for an additional 24 hours prior

to harvesting. The HEK293T cell line used in this study was obtained from ATCC (catalog # CRL-3216). The cell line was not further authenticated, and was not tested for mycoplasma contamination.

Cloning and expression of hDRD2^{EM} and G_i heterotrimer

The designed hDRD2^{EM} construct contains 5 mutations: T205$^{5.54}$I, M374$^{6.36}$L, V378$^{6.40}$Y, V381$^{6.43}$L and V421$^{7.48}$I. Residues 1–29 were replaced with T4 lysozyme followed by a 2-residue (AlaAla) linker, and residues 222–360 in ICL3 were replaced with residues LVNTN, as designed in the optimized 7-residue ICL3 described above (with one wild-type amino acid flanking each side of the insertion). The resulting construct was cloned into a modified pFastBac baculovirus expression vector with a HA signal sequence followed by a FLAG tag at the N terminus. A dominant-negative rat $G\alpha_{i1}$ (DNGα_{i1}) was made by incorporating 3 mutations S47N[49], G203A[50] and E245A[51] which can stabilize the GPCR-G protein complex as previously reported[52]. Rat $G\alpha_{i1}$ only differs from human $G\alpha_{i1}$ by a single residue at position 98 in the AH domain where it is Ala in rat and Ser in human. A second pFastBac baculovirus was made with rat DNGα_{i1}. An additional pFastBac-Dual baculovirus was made with human $G\beta_1$ and human $G\gamma_2$ genes. An 8xHis tag was placed at the N-terminus of $G\gamma_2$. hDRD2^{EM}, DNGα_{i1}, $G\beta_1$, and His_8-tagged $G\gamma_2$ were co-expressed in *Spodoptera frugiperda (Sf9)* with the addition of all three baculoviruses (ratio of 1 hDRD2^{EM}:2 DNGα_{i1}:1 $G\beta_1G\gamma_2$) to *Sf*9 cells at a density of 3×10^6 ml^{-1} with 1 μM bromocriptine mesylate (Sigma) added to the media during growth. After 48 hours, cells were harvested and stored at −80 °C for future use. The *Sf9* cell line used in this study was obtained from Expression Systems Inc. (catalog # 94–001S). The cell line was not further authenticated, and was not tested for mycoplasma contamination.

Cloning, expression and purification of scFv16

The single chain antibody scFv16 was described in previous GPCR-G_i heterotrimer complexes[12,13]. A synthesized scFv16 DNA fragment was cloned into a modified pFastBac baculovirus expression vector (Invitrogen) with a melittin signal sequence at the N terminus and a decahistidine tag at the C terminus. The resulting construct was expressed in *Sf9* cells with the Bac-to-Bac system (Invitrogen). scFv16 was purified as previously described[12]. In brief, the secreted scFv16 in the cell culture media was separated from *Sf*9 cells by centrifugation and 10 mM Tris buffer pH 8.0 was added for balancing pH. Then 1 mM Ni_2SO_4 and 5 mM $CaCl_2$ were added to quench chelating agents. The solution containing scFv16 was loaded onto Ni-NTA affinity resin by a siphon. The column was washed with 20 column volumes of buffer consisting of 50 mM Hepes, pH 7.4, 150 mM NaCl and 10 mM imidazole. Protein was eluted from Ni-NTA resin with 10 column volumes of buffer consisting of 50 mM Hepes, pH 7.4, 150 mM NaCl and 250 mM imidazole. The eluate was concentrated and run on a Superdex 200 gel filtration column. The peak corresponding to monomeric scFv16 was collected, concentrated and frozen until further use.

Purification of the complex of hDRD2^{EM} and G_i heterotrimer

*Sf*9 cell pellets were resuspended and lysed in a hypotonic buffer consisting of 10 mM Hepes pH 7.4, 160 μg/ml benzamidine, 100 μg/ml leupeptin,1 mM $MgCl_2$, 0.1 mM TCEP, Apyrase (0.5 mU/ml, NEB) and 1 μM bromocriptine mesylate (Sigma) for 30 min at 4 °C.

Lysed cells were spun down and were homogenized using a Dounce tissue grinder (Wheaton) in a solubilization buffer consisting of 50 mM Hepes pH 7.4, 150 mM NaCl, 160 μg/ml benzamidine, 100 μg/ml leupeptin, 1 mM $MgCl_2$, 0.1 mM $MnCl_2$, 1% (w/v) lauryl maltose neopentyl glycol (LMNG, Anatrace), 0.1% Na Cholate, 0.1% cholesteryl hemi-succinate (CHS, Steraloids), 10% glycerol, 0.5 mM TCEP, apyrase (15 mU/ml, NEB), λ phosphatase (10 U/ml, NEB) and 10 μM bromocriptine mesylate (Sigma). Solubilization proceeded for 1 hour at 4 °C, followed by centrifugation at 35,000 rpm for 30 min at 4 °C. The supernatant was incubated with M1 anti-Flag affinity beads (Sigma) in batch-binding mode overnight at 4 °C in the presence of 2 mM $CaCl_2$. After binding, the M1 beads were spun down and transferred into a glass column. Then beads were washed with 10 volumes of buffer consisting of 50 mM Hepes, pH 7.4, 150 mM NaCl, 0.05% LMNG, 0.005% sodium cholate, 0.005% CHS, 5% glycerol, 1 mM $MgCl_2$, 2 mM $CaCl_2$, 0.5 mM TCEP and 5 μM bromocriptine mesylate. The complex was eluted from M1 beads with buffer consisting of 50 mM Hepes pH 7.4, 150 mM NaCl, 0.05% LMNG, 0.005% Na Cholate, 0.005% CHS, 5% glycerol, 0.5 mM TCEP, 5 μM bromocriptine mesylate, 200 μg/ml FLAG peptide and 5 mM EDTA. Finally, the eluate was concentrated and applied onto Superdex 200 size exclusion column (GE Healthcare). The peak corresponding to the $hDRD2^{EM}$-G_i heterotrimer complex was collected and mixed with scFv16 at a molar ratio 1:1.2 and incubated for 30 min on the ice. The isolated complex of $hDRD2^{EM}$, G_i heterotrimer and scFv16 was concentrated and used in further experiments.

Reconstitution into rHDL/nanodiscs

The complex of $hDRD2^{EM}$, G_i heterotrimer and scFv16 was inserted into reconstituted high density lipoprotein particles (rHDLs), commonly known as nanodiscs, as previously described[15]. In brief, the complex was mixed with MSP1D1 and a lipid mixture (POPC: POPG: Cholesterol = 3:2:1) at molar ratio 1:5:400 and the mixture was incubated for 1 hr at 4 °C. Bio-beads SM2 (50 mg/ml, Bio-Rad) were added into the mixture and incubated for 1 hr at 4 °C. The sample was transferred to fresh Bio-beads two additional times with the last incubation proceeding for 8 hr. The reconstitution mixture was spun down and the supernatant was loaded onto an M1 anti-Flag affinity column to remove empty nanodiscs. The eluate from the M1 beads was concentrated and applied onto a Superose 6 gel filtration column (GE Healthcare) (Extended Data Fig. 4a). The peak corresponding to the complex reconstituted in rHDL/nanodisc was collected and analyzed by SDS-PAGE gel electrophoresis (Extended Data Fig. 4b).

Cryo-EM data acquisition

The $hDRD2^{EM}$-G_i-scFv16 rHDL/nanodisc complex was concentrated to 6 mg/ml and supplemented with 2 mM fluorinated fos-choline-8 (Anatrace) immediately prior to freezing. Cryo-EM grids were prepared by applying 3.5 μl of this sample to glow-discharged Quantifoil R1.2/1.3 300-mesh gold holey carbon grids (Quantifoil Micro Tools GmbH, Germany), blotted for 4.5 sec under 90% humidity at 4 °C and plunge frozen in liquid ethane cooled by liquid nitrogen using a Mark IV Vitrobot. Cryo-EM grids were first imaged on a Talos Arctica microscope (FEI) operated at 200kV with a K3 direct electron detector (Gatan) using a Volta phase plate following a protocol as previously described[53]. SerialEM software was used for automated data collection. Images were recorded at a nominal

magnification of ×45,000, corresponding to a pixel size of 0.4385 and defocus set at 0.75 μm. Each stack image was dose-fractionated to 50 frames for a total of 2.5 s under a dose rate of 22 $e^-/Å^2/s$, resulting in a total dose of 55 $e^-/Å^2$. For high-resolution data collection, images were recorded on a Titan Krios microscope (FEI) operated at 300kV with a K3 direct electron detector (Gatan) in super-resolution mode using a slit width of 20 eV on a GIF-Quantum energy filter. SerialEM[54] was used for automated data collection. Images were recorded at a nominal magnification of ×105,000, corresponding to a pixel size of 0.415 Å and the defocus set in a range from 1.5 to 2.5 μm. Each stack image was dose-fractionated to 40 frames for a total of 2 s under a dose rate of 32 $e^-/Å^2/s$, resulting in a total dose of 64 $e^-/Å^2$.

Image processing

All datasets were processed in Relion 3.0[55] following the same general protocol as previously described[56]. 697 dose-fractioned images collected on a Talos Arctica microscope were gain normalized, 2 × 2 Fourier binned, motion corrected, dose-weighted, and summed using MotionCorr2[57]. Contrast transfer function parameters were estimated using GCTF[58]. Approximately 1,000 particles were picked manually and subjected to 2D classification. Representative projections of the complex were selected as templates for automated particle picking from all images. The 233,645 extracted particles were 4 × 4 binned and subjected to 2D classification. 2D classes displaying clear domain boundaries in complexes were picked and used to generate an ab initio model in Relion. A total of 42,956 particles were finally selected for 3D classification using the ab initio model as the reference. After 3D classification, the classes showing good secondary structure features were selected, combined and re-extracted at the original pixel size of 0.877 Å. After 3D refinement, the resulting 3D reconstitution from 11,290 particles yielded a map at 19 Å resolution (gold-standard FSC criterion[59]). The same procedure was applied to process data collected on Titan Krios. 9,760 dose-fractioned images collected on Titan Krios were gain normalized, 2 × 2 Fourier binned, motion corrected, dose-weighted, and summed using MotionCor2[57]. Contrast transfer function parameters were estimated using GCTF[58]. Approximately 1,000 particles were picked manually and subjected to 2D classification. Representative projections of the complex were selected as templates for automated particle picking from all images. The 2,001,023 extracted particles were 4 × 4 binned and subjected to 2D classification. A total of 1,341,844 particles were finally selected for 3D classification using the map reconstituted from the data collected on Talos Arctica as the reference. After 2 rounds of 3D classification, the classes showing good secondary structure features were selected, combined and re-extracted at the original pixel size of 0.83 Å. After 3D refinement and postprocessing, the resulting 3D reconstitution from 783,984 particles yielded a map at 3.8 Å resolution (gold-standard FSC criterion). To identify a subset of these particles with better density in the transmembrane domain, we carried out a focused 3D classification[60] subtracting the density of T4 lysozyme, AH domain in the $G\alpha_{i1}$ subunit, scFv16 and the belt-like density from the MSP1D1 nanodisc. The subsequent 3D classification separated out a class with 43,733 particles showing better density in the transmembrane domain (Extended Data Fig 6a). The selected particles from this class were subjected to 3D refinement and postprocessing yielding a map with 3.7 Å resolution. To improve the density of the AH domain in the $G\alpha_{i1}$ subunit, we carried out another focused 3D classification subtracting the

density of T4 lysozyme, DRD2, scFv16 and the belt-like density from the MSP1D1 nanodisc. The subsequent 3D classification separated out a class with 58,356 particles showing partial secondary structures within the AH domain (Extended Data Fig. 6b), which allowed us to dock a crystal structure of the AH domain (PDB: 1GP2).

Model building

The Cryo-EM structure of the μOR–G_i complex with scFv16[4] (PDB: 6ddf) was used as an initial model for model rebuilding and refinement. A polyalanine model was made from the μOR structure, and together with structures of G_i and sFv16 (PDB: 6ddf) was docked into the EM electron density map in Chimera[61]. The resulting model was subjected to autobuilding in Buccaneer[62], iterative building in Coot[63] and refinement in Phenix.real_space_refine[64]. Initial coordinates and refinement parameters for the ligand bromocriptine were prepared with Grade web server (http://grade.globalphasing.org). The structure of the AH domain from the GDP-bound G_i crystal structure[36] (PDB: 1GP2) was docked into the focused refined EM map. Manual editing in Coot and refinement in Phenix.real_space_refine were carried out to reduce the clashes of the docked AH domain with the $G\alpha_i$ Ras-like domain and Gβ subunit. The density of T4 lysozyme was poor and not modelled. FSC curves were calculated based on the model and maps in Phenix.validatiion_cryoem (Extended Data Fig. 6c). Representative cryo-EM density for the receptor is displayed in Extended Data Fig. 6d. MolProbity[65] was used to evaluate the final structures. In the Ramachandran plot, 97.7% and 2.3% of residues were in favored and allowed regions, respectively. The statistics for data collection and refinement are included in Extended Data Table 1. The consensus cryo-EM density map and two focused maps have been deposited in the Electron Microscopy Data Bank under accession codes EMD-21243, EMD-21244, and EMD-21245. Atomic coordinates have been deposited in the PDB under accession code 6vms.

Radioligand binding assays

Membranes were prepared from *Sf9* cells co-infected with $G\alpha_{i1}\beta_1\gamma_2$ and wild-type human $DRD2_{long}$ ($DRD2^{WT}$) as described[31]. Membranes (7–10 μg) were pretreated with or without antibody fragment scFv16 (1 μg/10 μg membranes) for 30 min at room temp and then incubated for 2 hr at 30°C in binding buffer (20 mM HEPES, pH 7.4, 100 mM NaCl, 1 mM ascorbic acid, 0.001% BSA, 100 nM GDP) and 0.03 – 1.6 nM [^{3}H]spiperone (for saturations) or with 0.13 nM [^{3}H]spiperone (for competitions) along with varying concentrations of dopamine (or with 20 μM (+)butaclamol to determine non-specific binding). Samples were subject to rapid filtration through GF/B Unifilter™ plates (Packard) and rinsed with ice cold binding buffer to remove free [^{3}H]spiperone. Filter plates were dried before adding Microscint 0™ (Perkin Elmer) and counting bound [^{3}H]spiperone using a TopCount™ (Perkin Elmer). All data were analyzed using Prism (Graphpad Software Inc, San Diego CA).

[^{35}S]GTPγS binding assay

Membranes were prepared from *Sf*9 cells expressing $G\alpha_{i1}\beta_1\gamma_2$ and hDRD2 wild-type or $hDRD2^{EM}$. Typically, membranes (~30 μg) were pretreated with GDP (final assay concentration of 1 μM) in G assay buffer (20 mM HEPES, pH 7.4, 100 mM NaCl, 10 mM

$MgCl_2$, and 1 mM ascorbic acid) and different concentrations of ligand(s) for 10 min at room temperature before adding [^{35}S]GTPγS (for a final concentration of 0.1 nM). The assay was incubated at 30°C for 1 hr before stopping by rapid filtration through GF/B Unifilter plates and washing with ice-cold assay buffer. Filter plates were dried before adding Microscint 0™ and counting bound [^{35}S]GTPγS using a TopCount™ (Perkin Elmer).

Receptor stability

For stability experiments, partially purified DRD2 receptor (or mutant) was prepared from membranes from transfected cells expressing either hDRD2^{WT} or hDRD2^{EM} as previously described[48]. Briefly, transfected HEK293 cells were gently harvested in PBS solution, pelleted by low speed centrifugation and resuspended in cold hypotonic buffer (1 mM Tris-HCL, pH 6.8, 10 mM EDTA, protease inhibitor cocktail). Cells were disrupted through a 26-gauge needle three times and the lysate was layered onto a 38% sucrose solution in buffer A (150 mM NaCl, 1 mM MgCl, 10 mM EDTA, 20 mM Tris-HCl, pH 6.8, protease inhibitors) and spun at 15,000 rpm for 20 minutes at 4 °C using a swinging bucket rotor (SW28). The fluffy interface band containing enriched membranes were diluted in Buffer A and pelleted by ultracentrifugation. Membrane pellets were resuspended in Buffer A, flash frozen in liquid N_2 and stored at −80 °C until further use. Membranes were rapidly thawed, resuspended in 50 mM Tris-HCl, pH 7.4, 150 mM NaCl (plus protease inhibitors) and membrane proteins were solubilized in 1% n-dodecylmaltoside (DDM) for one hour at 4 °C. Insoluble material was removed by ultracentrifugation. Solubilized DRD2 (or mutant) were enriched using anti-HA agarose beads (Pierce/Thermo Scientific) at 4°C. The beads were washed with TBS with 0.1% DDM wash buffer three times and HA-tagged receptor variants were eluted with HA peptide (1 mg/mL in TBS with 0.1% DDM).

To measure apparent receptor half-life, 10 nM partially purified DRD2^{WT} or DRD2 with 5 designed mutations and designed truncated ICL3 were pre-incubated at 37 °C for 0–75 minutes prior to the addition and short preincubation with reaction mixture containing 20 μM [^{35}S]GTPγS and 20 μM dopamine in a buffer containing 50 mM Tris-HCl, pH 7.2, 100 mM NaCl, 4 mM $MgCl_2$ and 1 mM dithiothreitol. [^{35}S]GTPγS binding was initiated with the addition of 4 μM G_{i2} (purified as described previously[48]) for 30 min at room temperature. Reaction was terminated by rapid filtration on nitrocellulose filterplates. Microscint 0™ was added to dried filterplates and counted on a Topcount™ (Perkin Elmer).

To assess the apparent melting temperatures, partially pure receptor preparations (10 nM) were pre-incubated at varying temperatures (0 – 50°C) for 30 min. Functional receptor was determined by assessing radioligand binding using [^{3}H]dopamine in a buffer containing 50 mM Tris-HCl, pH 7.2, 100 mM NaCl and 4 mM $MgCl_2$. Reaction was terminated by rapid filtration on nitrocellulose filterplates. Microscint 0™ was added to dried filterplates and counted on a Topcount™ (Perkin Elmer). Apparent melting temperatures and active state half-life curves were fitted using Graphpad Prism version 8 (Graphpad Software Inc., San Diego CA).

Data Availability

Structural data have been deposited in the Protein Data Bank (PDB) with coordinate accession number 6vms, and maps have been deposited in the Electron Microscopy Data Bank (EMDB) with accession numbers EMD-21243, EMD-21244, and EMD-21245. All other data generated or analyzed during this study are included in this published article or are available from the corresponding authors on reasonable request.

Extended Data

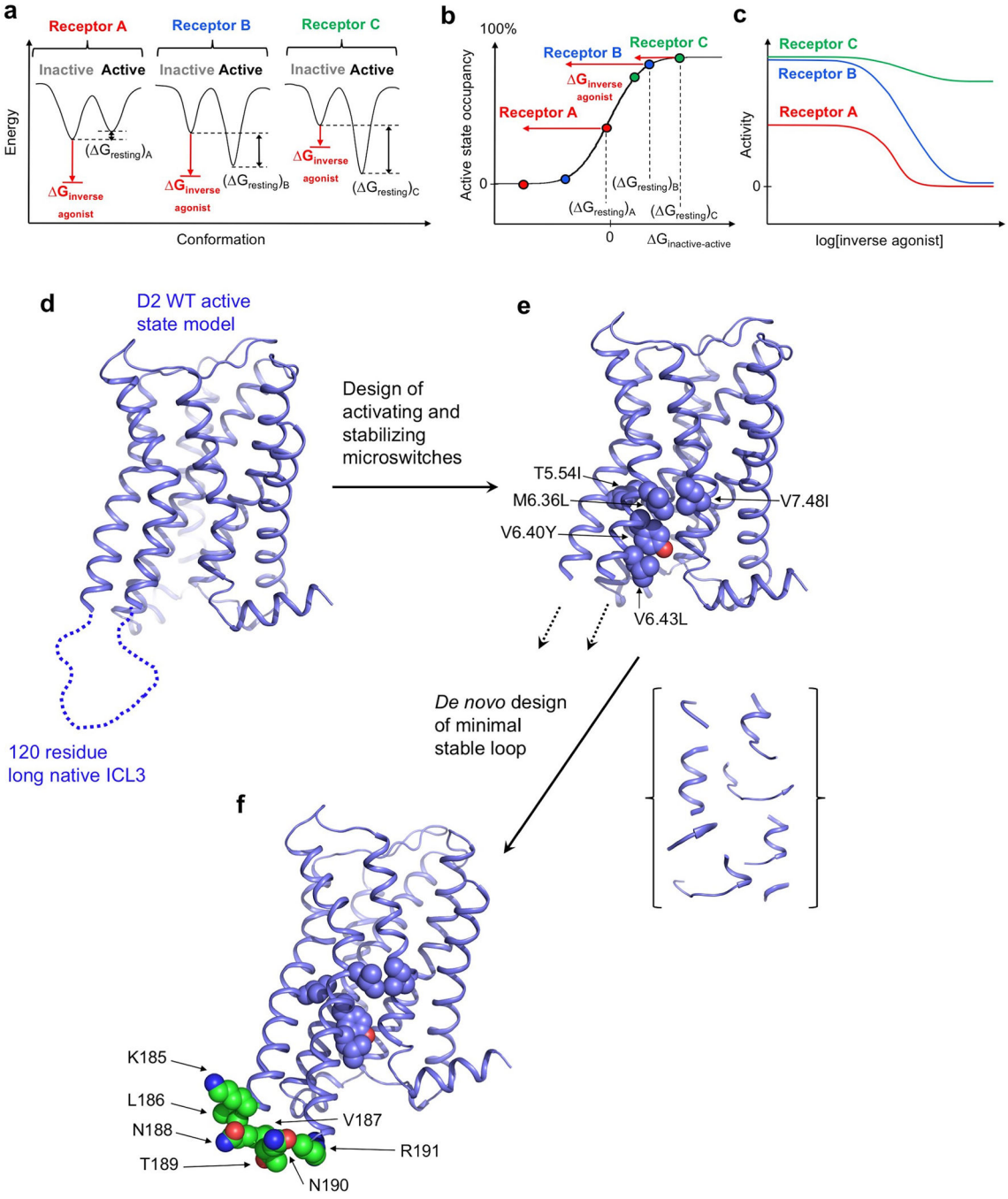

Extended Data Figure 1.

Rational design of receptor variants shifted in the active state. (a) Energy landscape of 3 receptor variants with various energy differences in the resting (ligand-free) state $\Delta G_{resting}$, in the allosteric coupling controlling the inverse agonist efficacy $\Delta G_{inverse\ agonist}$ and the stabilization of the receptor inactive state upon ligand stimulus. (b) Active state occupancy as a function of $\Delta G_{resting}$ and $\Delta G_{inverse\ agonist}$ (the energy of inverse agonist binding), as determined by the Boltzmann law. (c) Sensitivity of the receptors to inverse agonist binding. (d-f). Rational design of DRD2 receptor stabilized in the active state. (d) DRD2 WT active

state homology model. The 120 residue long intracellular loop 3 (ICL3) is represented as a dotted blue line. (e) DRD2 designed with residue microswitches shown in spheres stabilizing selectively the active state structure. (f) DRD2 further stabilized in the active state through a *de novo* designed 7-residue stable ICL3.

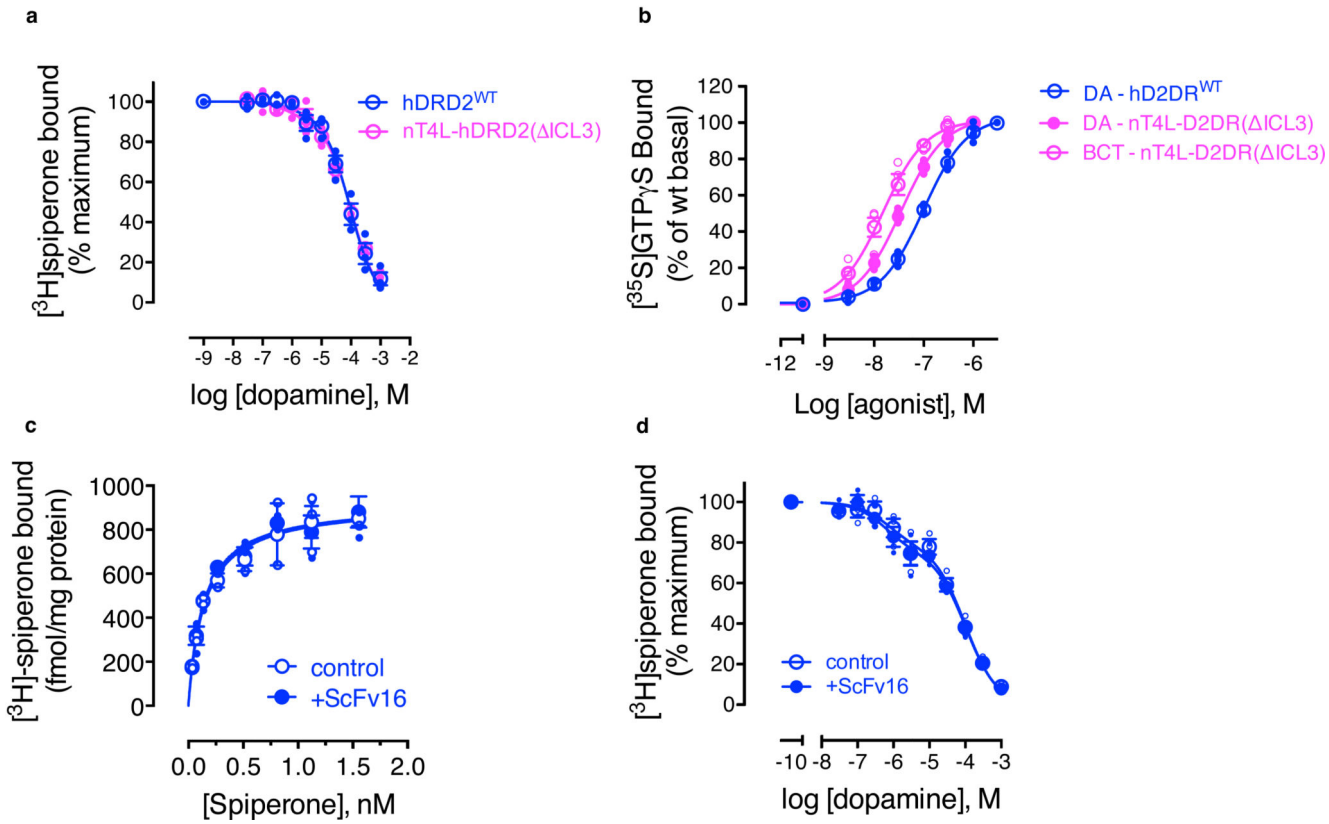

Extended Data Figure 2.

Effect of T4L, modified ICL3, and scFv16 on hDRD2^{WT} ligand binding properties. (a) Competition binding of dopamine for [^{3}H]spiperone on membranes containing human DRD2 wild type (hDRD2^{WT}, blue) or human DRD2 modified with N-terminal T4L and *de novo* designed ICL3, nT4L-hDRD2(ΔICL3) (magenta). Log K_i ± S.E.M. = −4.6 ± 0.04 for hDRD2^{WT}. Log K_i ± S.E. = −4.6 ± 0.04 for nT4L-hDRD2(ΔICL3). n = 4 biologically independent experiments on *Sf9* cell membranes. (b) Agonist-stimulated [^{35}S]GTPγS binding of nT4L-hDRD2(ΔICL3) (magenta symbols) compared to hDRD2^{WT} (blue symbols). Dose-response using dopamine (closed magenta) or bromocriptine (open magenta) show log EC_{50} ± S.E.M. = −7.5 ± 0.02 M and −7.8 ± 0.06 M, respectively, for nT4L-hDRD2(ΔICL3) compared to log EC_{50} ± S.E.M. −7.0 ± 0.02 M for dopamine on hDRD2^{WT} (open blue). n = 3 biologically independent experiments on HEK293T cell membranes. c) Saturation binding of [^{3}H]spiperone to membranes containing DRD2^{WT} with or without scFv16. K_d ± S.E.M. = 0.15 nM ± 0.03 nM for control. K_d ± S.E.M. = 0.14 nM ± 0.02 nM with scFv16. n = 4 biologically independent experiments on *Sf9* cell membranes. (d) Competition binding of dopamine for [^{3}H]spiperone on membranes containing DRD2^{WT} with or without scFv16. Log K_{high} ± S.E.M. = −6.4 ± 0.3 and Log K_{low} ± S.E.M. = −4.3 ± 0.08 for control. Log K_{high} ± S.E.M. = −6.5 ± 0.2 and Log K_{low} ± S.E.M. = −4.3 ± 0.07 with scFv16. n = 4 biologically independent experiments on *Sf9* cell membranes. In all panels, each data point is displayed as mean with error bars showing ± S.E.M., with individual data points for each repeat represented in small symbols.

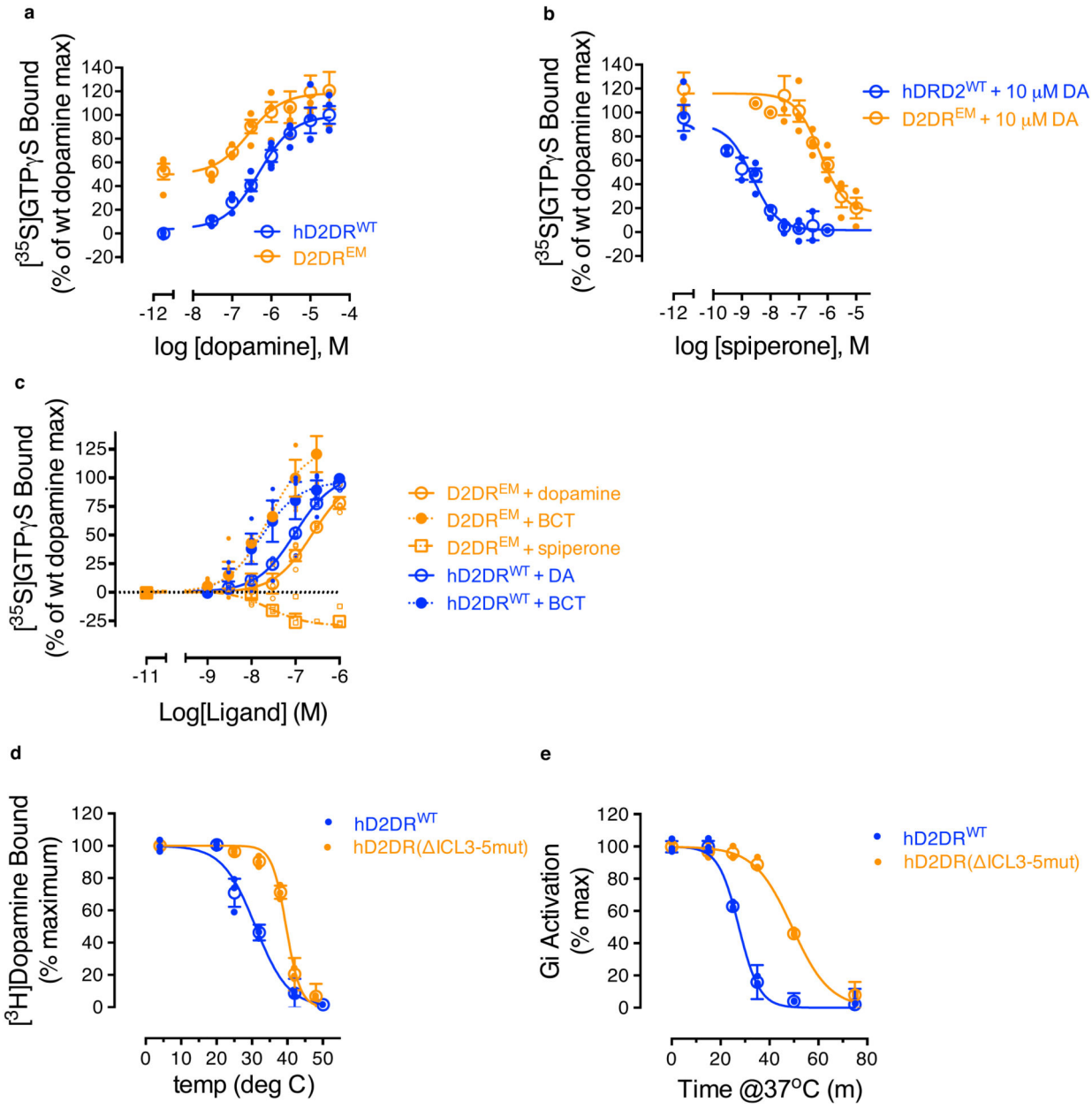

Extended Data Figure 3.

Function and thermostability of hDRD2^{EM}. (a) G_i stimulation by dopamine in *Sf9* cells transformed with G_i and hDRD2 baculoviruses. Log EC_{50} ± S.E.M. = −6.3 ± 0.1 for hDRD2^{WT} (blue). Log EC_{50} ± S.E.M. = −6.6 ± 0.3 for hDRD2^{EM} (orange). n = 4 biologically independent experiments on *Sf9* cell membranes. (b) Inhibition of dopamine-stimulated (10 μM) G_i activation by the inverse agonist spiperone. Log IC_{50} ± S.E.M = −8.6 ± 0.1 for hDRD2^{WT} (blue). Log IC_{50} ± S.E.M = −6.3 ± 0.2 for hDRD2^{EM} (orange). n = 4 biologically independent experiments on *Sf9* cell membranes. (c) Modulation of basal G_i activation by dopamine (open), bromocriptine (closed) or spiperone (squares) with the hDRD2^{EM} (orange symbols) relative to hDRD2^{WT}(blue symbols). Log EC_{50} ± S.E.M. for dopamine (−6.6 ± 0.2 M), bromocriptine (−7.6 ± 0.1 M) and spiperone (−7.6 ± 0.2 M) for

hDRD2^{EM}. Log EC_{50} ± S.E.M. for dopamine (−7.0 ± 0.1 M) and bromocriptine (−7.8 ± 0.2 M) for hDRD2^{WT}. n = 3 biologically independent experiments on *Sf9* cell membranes. (d) Apparent functional stability of agonist-bound hDRD2 constructs assessed by measuring the fraction of partially-purified receptor activating G_i as a function of incubation time at 37ºC. Half-life ± S.E.M.= 27.6 min ± 1.0 min for hDRD2^{WT} (blue). Half-life ± S.E.M. = 49.3 min ± 1.1 min for hDRD2 with 5 designed mutations and designed truncated ICL3 (orange). n = 3 biologically independent experiments (e) Apparent thermostability of agonist-bound hDRD2 constructs assessed by measuring the fraction of partially-purified receptor binding agonist as a function of temperature. T_m ± S.E.M.= 30.9 °C ± 0.9 °C for hDRD2^{WT}(blue). T_m ± S.E.M. = 39.6 °C ± 0.3 °C for hDRD2 with 5 designed mutations and designed truncated ICL3 (orange). n = 3 biologically independent experiments. In all panels, each data point is displayed as mean with error bars showing ± S.E.M., with individual data points for each repeat represented in small symbols.

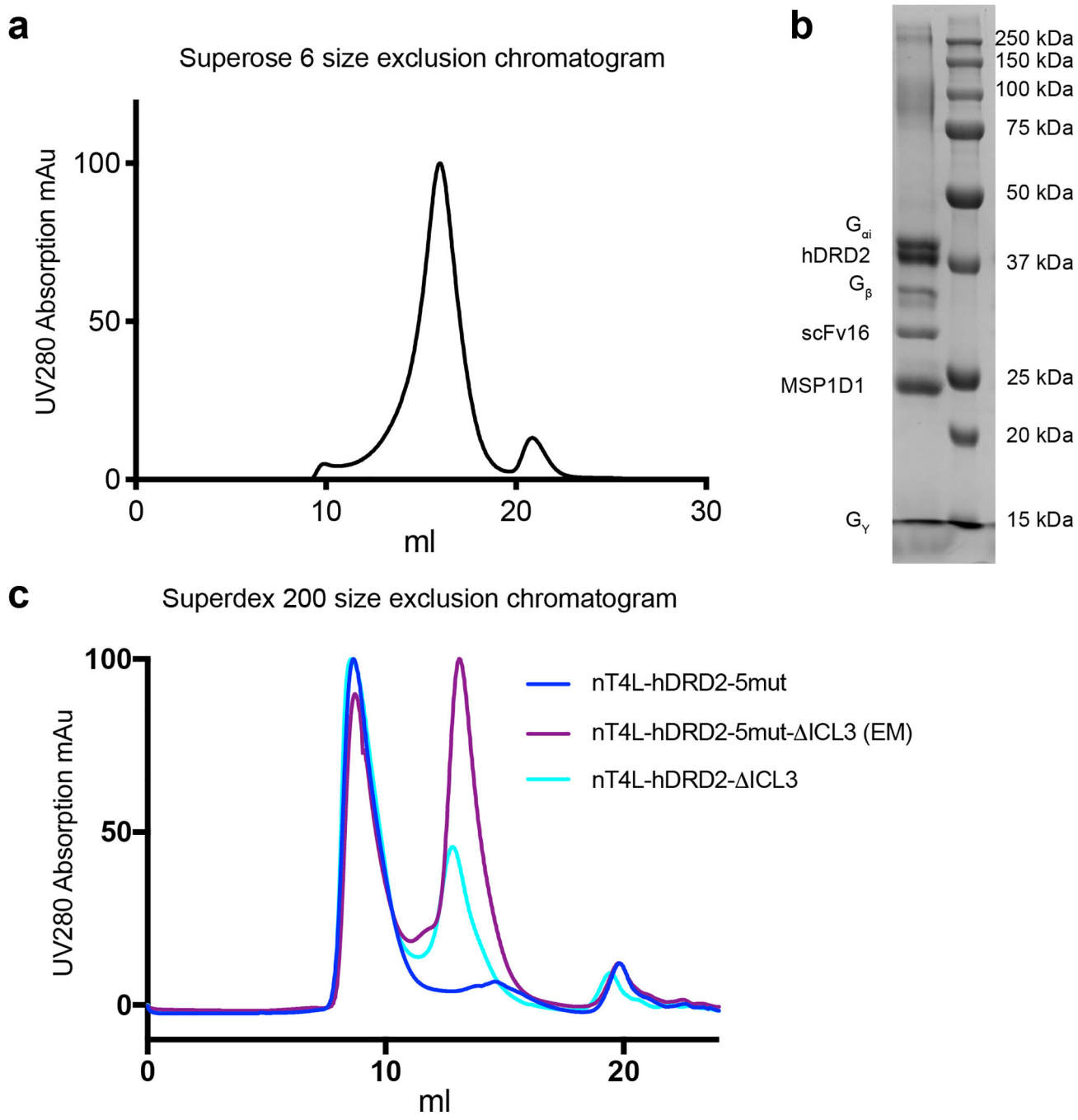

Extended Data Figure 4.

Purification and reconstitution of the hDRD2^{EM}-G_i complex. (a) Superose 6 gel filtration profile of hDRD2^{EM}-Gi-scFv16-HDL purified by M1 FLAG affinity chromatography. (b) Coomassie stained PAGE of the isolated peak fraction from gel filtration. (c) Overlaid Superose 200 gel filtration profiles (in LMNG detergent) of different hDRD2 constructs purified by M1 FLAG chromatography with saturating bromocriptine present. nT4L-hDRD2–5mut has the 5 thermostabilizing mutations of the EM construct, but has full-length ICL3. nT4L-hDRD2-ΔICL3 has the wild-type TM region (no mutations) but the truncated

ICL3. Receptors were purified as in Methods, but in the absence of co-transduced G protein baculovirus.

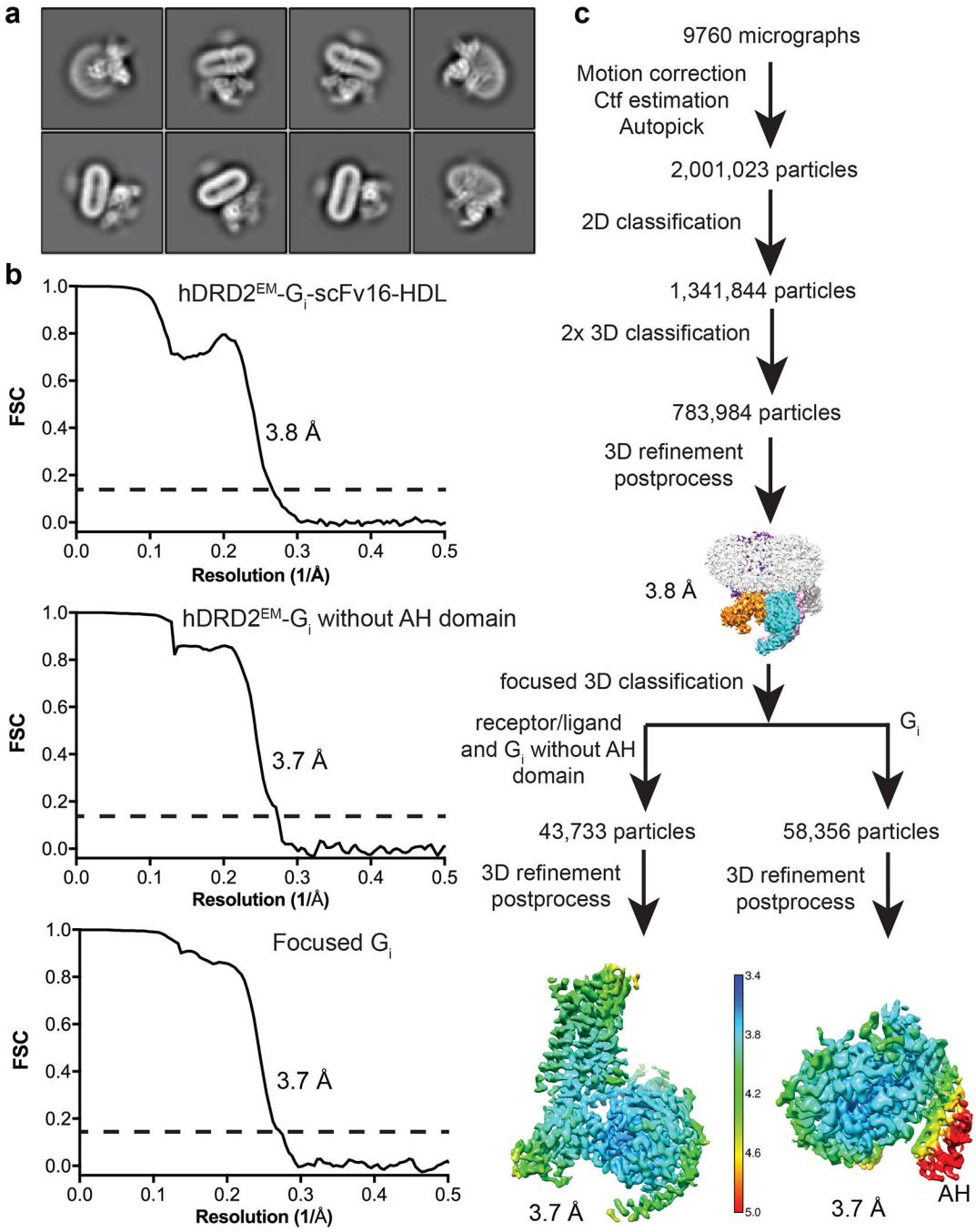

Extended Data Figure 5.

Cryo-EM data analysis. (a) Representative 2D class averages. (b) Gold-standard FSC curves of the 3D reconstructions. (c) Image processing procedure with the final maps colored based on local resolution.

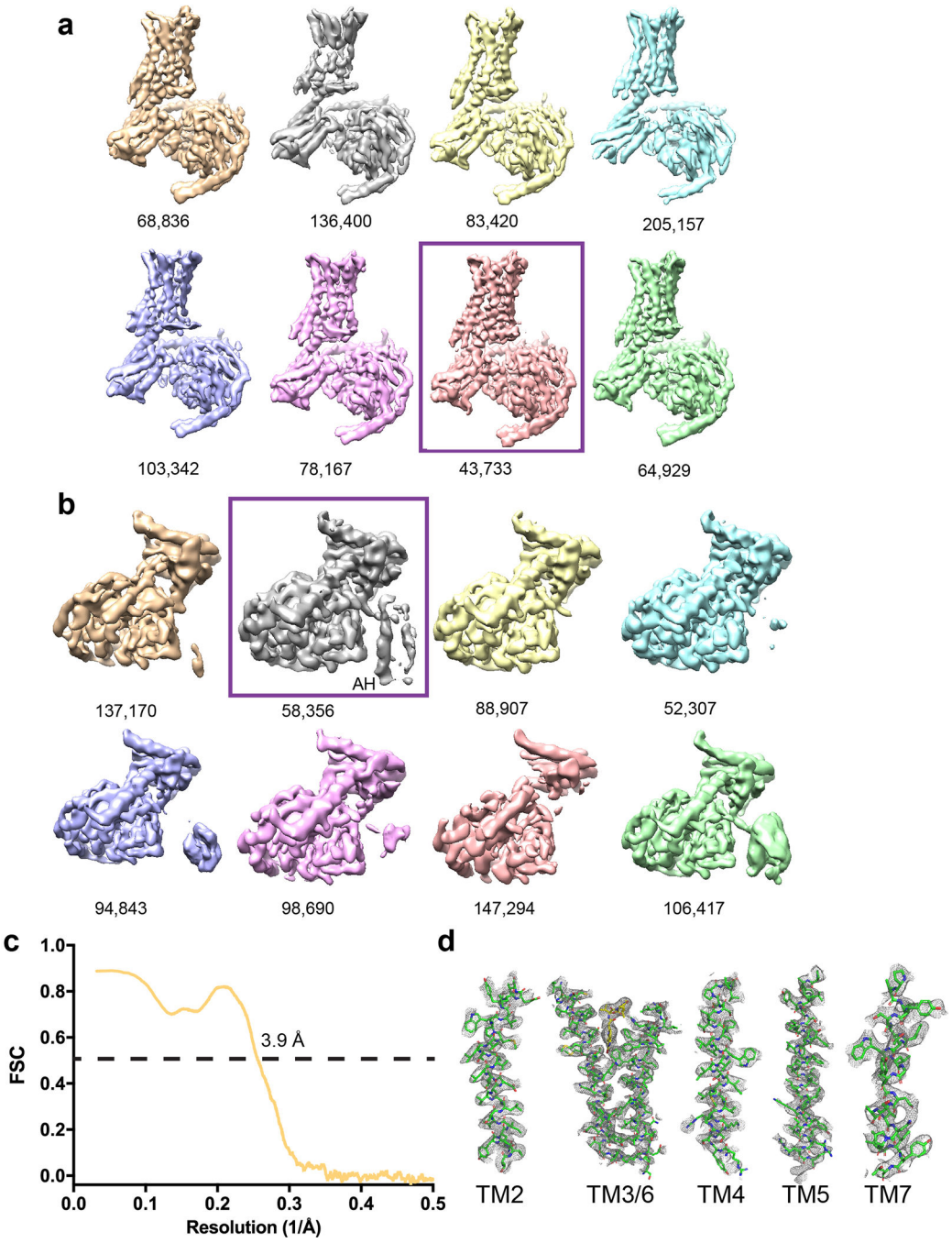

Extended Data Figure 6.

3D classification with signal subtraction, model validation and representative map density. (a) Focused 3D classification subtracting T4L, AH domain, scFv16, and nanodisc density. (b) Focused 3D classification subtracting all but the G protein. (c) FSC curve showing the model-map correlation (focused map without T4L, AH domain, scFv16, and nanodisc density). (d) representative DRD2 TM and ligand density.

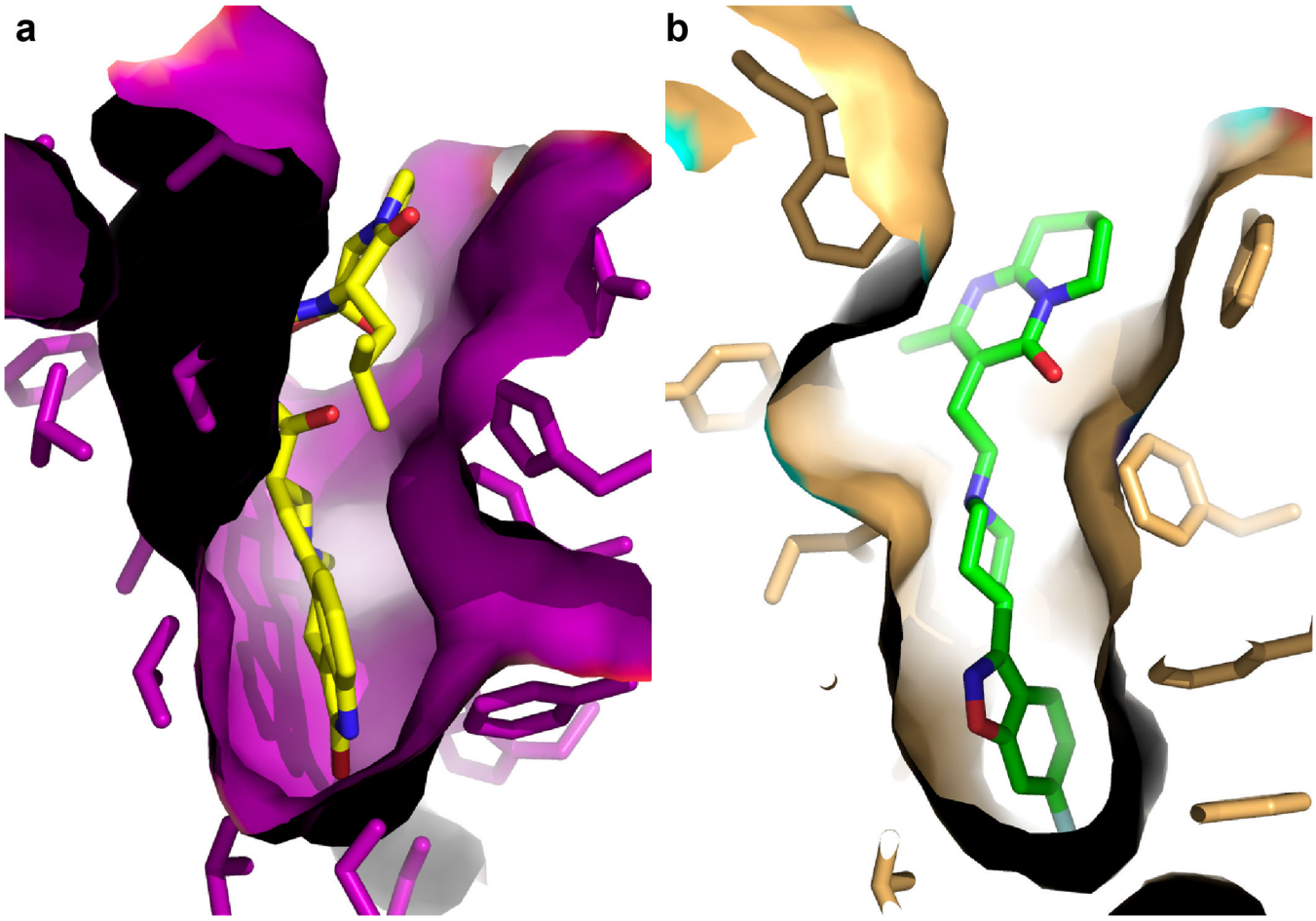

Extended Data Figure 7.

Surfaces of the orthosteric pocket in the active and inactive conformations of DRD2. (a) Solvent accessible surface for the active conformation (purple) bound to bromocriptine (yellow sticks). (b) Solvent accessible surface for the inactive conformation (orange) bound to risperidone (green sticks), showing the deeper subpocket (PDB 6cm4).

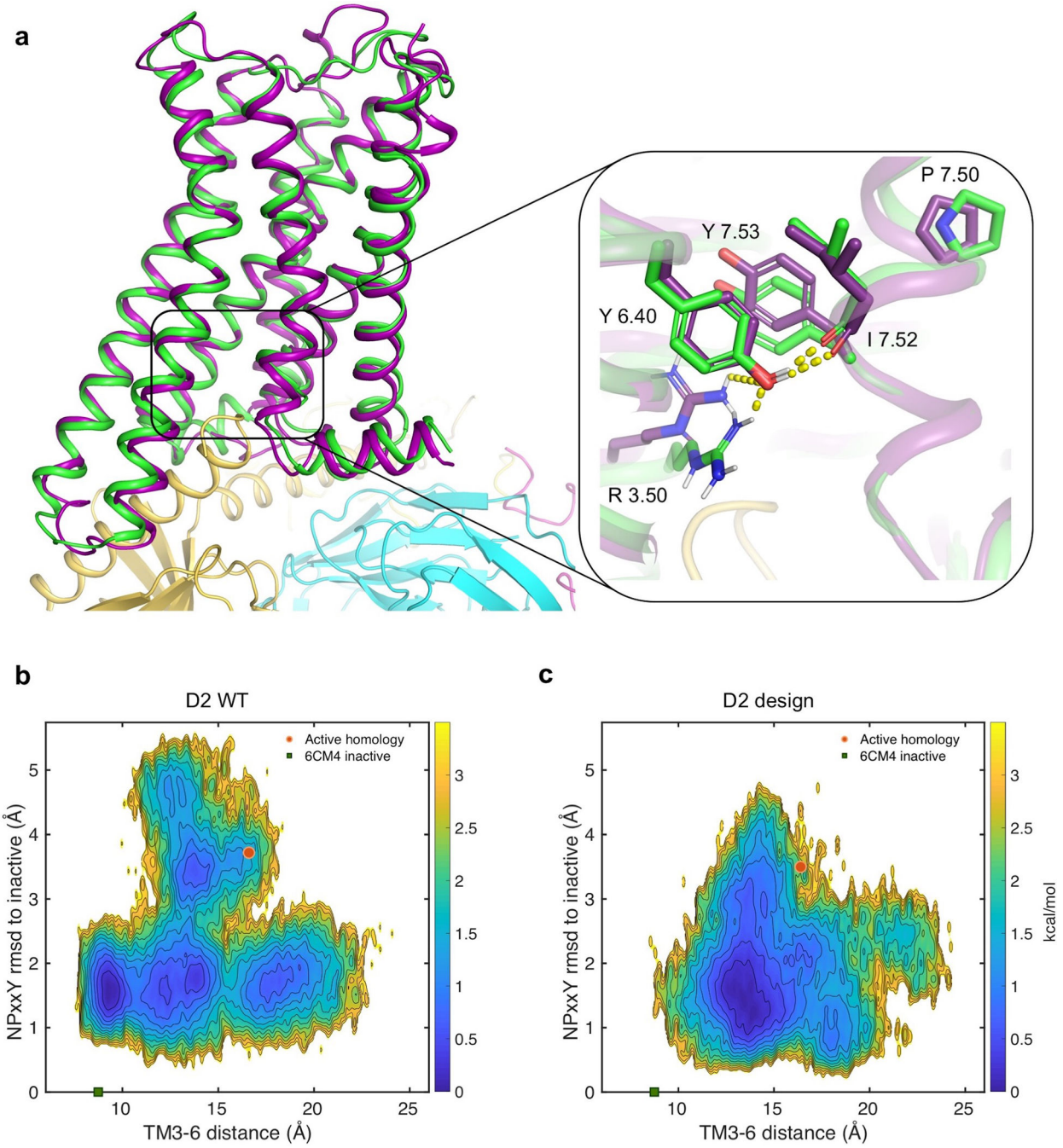

Extended Data Figure 8.

Interaction stabilizing the designed hDRD2^{EM} active state conformation. (a) Zoomed view of the TM6-TM7 interface on the cytoplasmic side of the receptor. Atomic interactions involving the designed Y6.40 were accurately predicted in the design model. The conformation of the R3.50 is displaced in the experimental structure due to the binding of $G_{i\alpha}$ which was absent in the model. Experimental structure is in purple and predicted DRD2 conformation is in green. (b, c) Conformational energy landscape of the WT (b) and designed (c) DRD2 receptors constructed from multiple all-atom MD simulation trajectories

of the receptor active state homology models (orange dot) in absence of bound agonist. The conformational space is reported along 2 canonical active state structure metrics (TM3–6 distance and NPxxY rmsd to inactive state). The DRD2 WT relaxes primarily to an inactive state conformation while the designed variant remains in partially active state conformation displaying large TM3–6 distance. The antagonist-bound DRD2 crystal structure (PDB 6CM4) is used as a reference for the inactive state (green square).

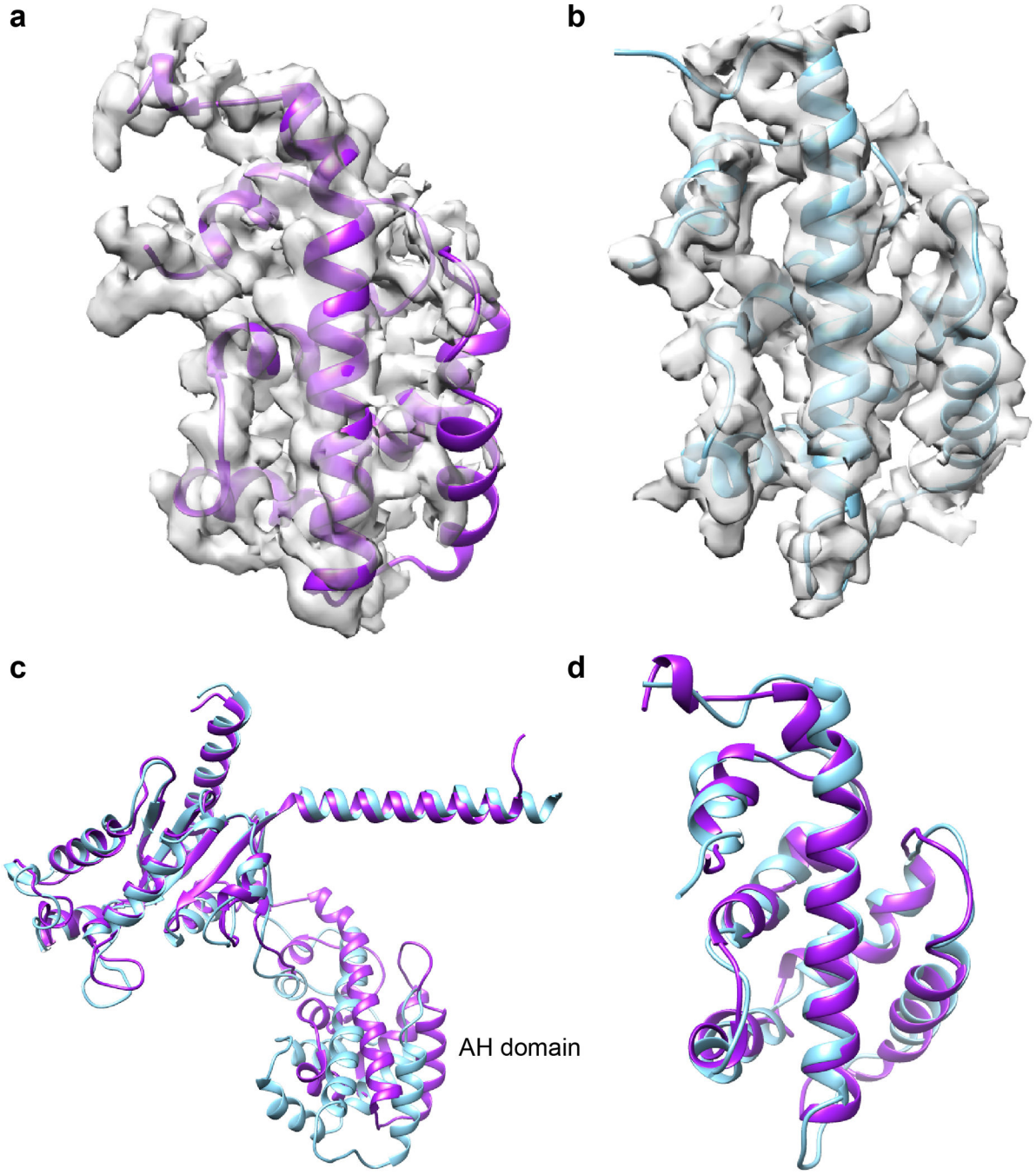

Extended Data Figure 9.

AH domain density and comparison with rhodopsin-G_i. (a) AH domain density in the current structure. (b) AH domain density in the rhodopsin-G_i complex (PDB 6cmo). (c) Alignment of $G\alpha_i$ subunit in hDRD2^{EM}-G_i (purple) and rhodopsin-G_i complex (blue). (d) Alignment of AH domain in hDRD2^{EM}-G_i (purple) and rhodopsin-G_i complex (blue).

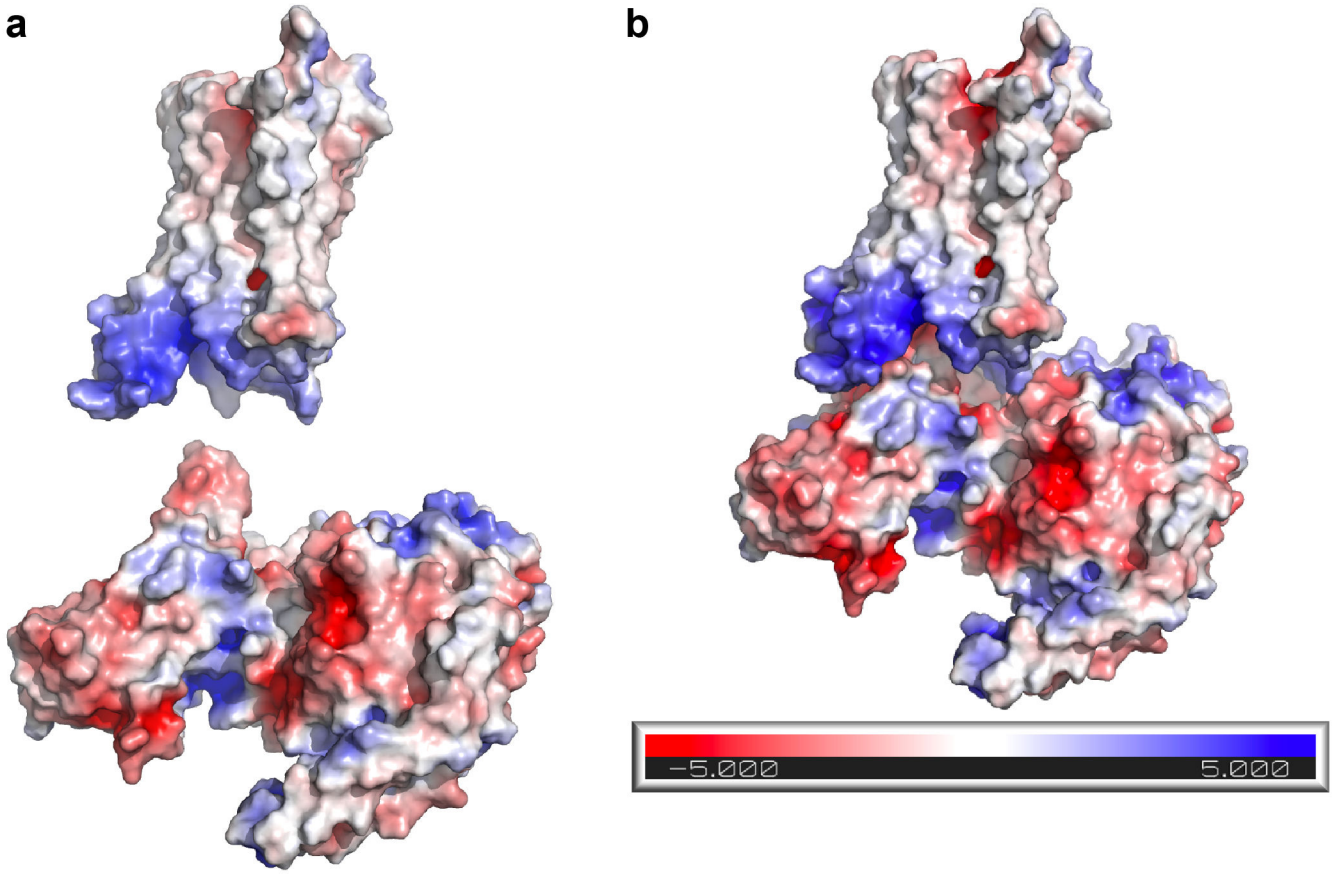

Extended Data Figure 10.

Electrostatic surfaces in the hDRD2^{EM}-G_i complex. (a) Surface potential of the DRD2 and G_i components shown separately. (b) Surface potential of the complex, with scale in eV. Calculation was done using the APBS plugin in Pymol.

Extended Data Table 1.

Cryo-EM data collection, refinement and validation statistics.

	hDRD2^{EM}-DNG$_{\alpha i1}$G$_{\beta 1}$G$_{\lambda 2}$-scFv16-HDL (EMD-21243)	**hDRD2^{EM}-DNG$_{\alpha i1}$G$_{\beta 1}$G$_{\lambda 2}$ focused (-nT4L, AH domain, scFv16 and HDL) (EMD-21244) (PDB 6vms)**	**DNG$_{\alpha i1}$G$_{\beta 1}$G$_{\lambda 2}$ focused (-Receptor, scFv16 and HDL) (EMDB-21245)**
Data collection and processing			
Magnification	105,000	105,000	105,000
Voltage (kV)	300	300	300
Electron exposure (e^{-}/Å^2)	64	64	64
Defocus range (μm)	1.5–2.5	1.5–2.5	1.5–2.5
Pixel size (Å)	0.83	0.83	0.83
Symmetry imposed	C1	C1	C1
Initial particle images (no.)	2,001,023	2,001,023	2,001,023

	hDRD2^{EM}-DNG$_{\alpha i1}$G$_{\beta 1}$G$_{\lambda 2}$-scFv16-HDL (EMD-21243)	**hDRD2^{EM}-DNG$_{\alpha i1}$G$_{\beta 1}$G$_{\lambda 2}$ focused (-nT4L, AH domain, scFv16 and HDL) (EMD-21244) (PDB 6vms)**	**DNG$_{\alpha i1}$G$_{\beta 1}$G$_{\lambda 2}$ focused (-Receptor, scFv16 and HDL) (EMDB-21245)**
Final particle images (no.)	783,984	43,733	58,356
Map resolution (Å)	3.8	3.7	3.7
FSC threshold	0.143	0.143	0.143
Refinement			
Initial model used (PDB code)	6dde, 1gp2		
Model Resolution (Å)	3.9		
FSC threshold	0.5		
Map sharpening *B* factor (Å^2)	−155		
Model composition			
Non-hydrogen atoms	8953		
Protein residues	1135 (8910 atoms)		
Ligands	1 (43 atoms)		
B factors (Å^2)			
Protein	81.57		
Ligand	67.82		
R.m.s deviations			
Bond lengths (Å)	0.005		
Bond angles (°)	0.703		
Validation			
MolProbity score	1.37		
Clashscore	5.56		
Poor rotamers (%)	0		
Ramachandran plot			
Favored (%)	97.68		
Allowed (%)	2.32		
Disallowed (%)	0		

Acknowledgements

Cryo-EM data were collected at the University of Texas Southwestern Medical Center Cryo-EM Facility, which is funded by the CPRIT Core Facility Support Award RP170644. We thank Elliott Ross for providing plasmids for G protein expression. This project was supported by the Edward Mallinckrodt, Jr. Foundation (Scholar Award to D.M.R.), the Welch Foundation (grant I-1770 to D.M.R, grant I-1944-20180324 to X.B.), the EPFL and the Ludwig Institute for Cancer research (to P.B.), the Virginia Murchison Linthicum Scholar in Medical Research at UTSW (X.B.), CPRIT (RR160082 to X.B.), and the National Institutes of Health (R01-GM097207 to P.B., R01-GM083118 to R.K.S.).

References

1. Sibley DR & Monsma FJ Molecular biology of dopamine receptors. Trends Pharmacol. Sci 13, 61–69 (1992). [PubMed: 1561715]
2. Seeman P Targeting the dopamine D2 receptor in schizophrenia. Expert Opin. Ther. Targets 10, 515–531 (2006). [PubMed: 16848689]

3. Michael Besser G, Pfeiffer RF & Thorner MO Anniversary Review: 50 years since the discovery of bromocriptine. Eur. J. Endocrinol 179, R69–R75 (2018). [PubMed: 29752299]
4. Dickson DW et al. Neuropathological assessment of Parkinson's disease: refining the diagnostic criteria. Lancet Neurol. 8, 1150–1157 (2009). [PubMed: 19909913]
5. Seo E-J, Sugimoto Y, Greten HJ & Efferth T Repurposing of Bromocriptine for Cancer Therapy. Front. Pharmacol 9, 1030 (2018). [PubMed: 30349477]
6. Madras BK History of the discovery of the antipsychotic dopamine D2 receptor: a basis for the dopamine hypothesis of schizophrenia. J. Hist. Neurosci 22, 62–78 (2013). [PubMed: 23323533]
7. Civelli O, Bunzow JR & Grandy DK Molecular diversity of the dopamine receptors. Annu. Rev. Pharmacol. Toxicol 33, 281–307 (1993). [PubMed: 8494342]
8. Moritz AE, Free RB & Sibley DR Advances and challenges in the search for D2 and D3 dopamine receptor-selective compounds. Cell. Signal 41, 75–81 (2018). [PubMed: 28716664]
9. Wang S et al. Structure of the D2 dopamine receptor bound to the atypical antipsychotic drug risperidone. Nature 555, 269–273 (2018). [PubMed: 29466326]
10. Chien EYT et al. Structure of the human dopamine D3 receptor in complex with a D2/D3 selective antagonist. Science 330, 1091–1095 (2010). [PubMed: 21097933]
11. Wang S et al. D4 dopamine receptor high-resolution structures enable the discovery of selective agonists. Science 358, 381–386 (2017). [PubMed: 29051383]
12. Koehl A et al. Structure of the μ-opioid receptor-Gi protein complex. Nature 558, 547–552 (2018). [PubMed: 29899455]
13. Krishna Kumar K et al. Structure of a Signaling Cannabinoid Receptor 1-G Protein Complex. Cell 176, 448–458.e12 (2019). [PubMed: 30639101]
14. Senogles SE, Amlaiky N, Falardeau P & Caron MG Purification and characterization of the D2-dopamine receptor from bovine anterior pituitary. J. Biol. Chem 263, 18996–19002 (1988). [PubMed: 3143721]
15. Whorton MR et al. A monomeric G protein-coupled receptor isolated in a high-density lipoprotein particle efficiently activates its G protein. Proc. Natl. Acad. Sci. USA 104, 7682–7687 (2007). [PubMed: 17452637]
16. Whorton MR et al. Efficient coupling of transducin to monomeric rhodopsin in a phospholipid bilayer. J. Biol. Chem 283, 4387–4394 (2008). [PubMed: 18033822]
17. Bayburt TH & Sligar SG Membrane protein assembly into Nanodiscs. FEBS Lett. 584, 1721–1727 (2010). [PubMed: 19836392]
18. Gao Y, Cao E, Julius D & Cheng Y TRPV1 structures in nanodiscs reveal mechanisms of ligand and lipid action. Nature 534, 347–351 (2016). [PubMed: 27281200]
19. Koehl A et al. Structural insights into the activation of metabotropic glutamate receptors. Nature 566, 79–84 (2019). [PubMed: 30675062]
20. Staus DP et al. Structure of the M2 muscarinic receptor-β-arrestin complex in a lipid nanodisc. Nature 41, 9–302 (2020).
21. Westfield GH et al. Structural flexibility of the G alpha s alpha-helical domain in the beta2-adrenoceptor Gs complex. Proc. Natl. Acad. Sci. USA 108, 16086–16091 (2011). [PubMed: 21914848]
22. Seeman P & Van Tol HH Dopamine receptor pharmacology. Trends Pharmacol. Sci 15, 264–270 (1994). [PubMed: 7940991]
23. Denisov IG, Grinkova YV, Lazarides AA & Sligar SG Directed self-assembly of monodisperse phospholipid bilayer Nanodiscs with controlled size. J. Am. Chem. Soc 126, 3477–3487 (2004). [PubMed: 15025475]
24. Rosenbaum DM et al. GPCR engineering yields high-resolution structural insights into beta2-adrenergic receptor function. Science 318, 1266–1273 (2007). [PubMed: 17962519]
25. Mansour A et al. Site-directed mutagenesis of the human dopamine D2 receptor. Eur. J. Pharmacol 227, 205–214 (1992). [PubMed: 1358663]
26. Wiens BL, Nelson CS & Neve KA Contribution of serine residues to constitutive and agonist-induced signaling via the D2S dopamine receptor: evidence for multiple, agonist-specific active conformations. Mol. Pharmacol 54, 435–444 (1998). [PubMed: 9687586]

27. Cho W, Taylor LP, Mansour A & Akil H Hydrophobic residues of the D2 dopamine receptor are important for binding and signal transduction. J. Neurochem 65, 2105–2115 (1995). [PubMed: 7595496]
28. Shi L & Javitch JA The second extracellular loop of the dopamine D2 receptor lines the binding-site crevice. Proc. Natl. Acad. Sci. USA 101, 440–445 (2004). [PubMed: 14704269]
29. Goldstein M et al. Interaction of pergolide with central dopaminergic receptors. Proc. Natl. Acad. Sci. USA 77, 3725–3728 (1980). [PubMed: 6932044]
30. Sibley DR & Creese I Interactions of ergot alkaloids with anterior pituitary D-2 dopamine receptors. Mol. Pharmacol 23, 585–593 (1983). [PubMed: 6223205]
31. DeVree BT et al. Allosteric coupling from G protein to the agonist-binding pocket in GPCRs. Nature 535, 182–186 (2016). [PubMed: 27362234]
32. McCorvy JD et al. Structure-inspired design of β-arrestin-biased ligands for aminergic GPCRs. Nat. Chem. Biol 14, 126–134 (2018). [PubMed: 29227473]
33. Sanchez-Soto M et al. A structural basis for how ligand binding site changes can allosterically regulate GPCR signaling and engender functional selectivity. Sci. Signal 13, eaaw5885 (2020). [PubMed: 32019899]
34. Latorraca NR, Venkatakrishnan AJ & Dror RO GPCR Dynamics: Structures in Motion. Chem. Rev 117, 139–155 (2017). [PubMed: 27622975]
35. Rasmussen SGF et al. Crystal structure of the β2 adrenergic receptor-Gs protein complex. Nature 477, 549–555 (2011). [PubMed: 21772288]
36. Wall MA et al. The structure of the G protein heterotrimer Gi alpha 1 beta 1 gamma 2. Cell 83, 1047–1058 (1995). [PubMed: 8521505]
37. Kang Y et al. Cryo-EM structure of human rhodopsin bound to an inhibitory G protein. Nature 558, 553–558 (2018). [PubMed: 29899450]
38. Mumby SM, Heukeroth RO, Gordon JI & Gilman AG G-protein alpha-subunit expression, myristoylation, and membrane association in COS cells. Proc. Natl. Acad. Sci. USA 87, 728–732 (1990). [PubMed: 2153964]
39. Mumby SM, Kleuss C & Gilman AG Receptor regulation of G-protein palmitoylation. Proc. Natl. Acad. Sci. USA 91, 2800–2804 (1994). [PubMed: 8146194]
40. Simonds WF, Butrynski JE, Gautam N, Unson CG & Spiegel AM G-protein beta gamma dimers. Membrane targeting requires subunit coexpression and intact gamma C-A-A-X domain. J. Biol. Chem 266, 5363–5366 (1991). [PubMed: 1706334]
41. Gallego C, Gupta SK, Winitz S, Eisfelder BJ & Johnson GL Myristoylation of the G alpha i2 polypeptide, a G protein alpha subunit, is required for its signaling and transformation functions. Proc. Natl. Acad. Sci. USA 89, 9695–9699 (1992). [PubMed: 1409685]
42. Sensoy O & Weinstein H A mechanistic role of Helix 8 in GPCRs: Computational modeling of the dopamine D2 receptor interaction with the GIPC1-PDZ-domain. Biochim. Biophys. Acta 1848, 976–983 (2015). [PubMed: 25592838]
43. Loisel TP et al. Activation of the beta(2)-adrenergic receptor-Galpha(s) complex leads to rapid depalmitoylation and inhibition of repalmitoylation of both the receptor and Galpha(s). J. Biol. Chem 274, 31014–31019 (1999). [PubMed: 10521499]
44. Krishna AG, Menon ST, Terry TJ & Sakmar TP Evidence that helix 8 of rhodopsin acts as a membrane-dependent conformational switch. Biochemistry 41, 8298–8309 (2002). [PubMed: 12081478]
45. Heijne G The distribution of positively charged residues in bacterial inner membrane proteins correlates with the trans-membrane topology. EMBO J. 5, 3021–3027 (1986). [PubMed: 16453726]
46. Dorairaj S & Allen TW On the thermodynamic stability of a charged arginine side chain in a transmembrane helix. Proc. Natl. Acad. Sci. USA 104, 4943–4948 (2007). [PubMed: 17360368]

Methods References

47. Feng X, Ambia J, Chen K-YM, Young M & Barth P Computational design of ligand-binding membrane receptors with high selectivity. Nat. Chem. Biol 13, 715–723 (2017). [PubMed: 28459439]
48. Chen K-YM, Keri D & Barth P Computational design of G Protein-Coupled Receptor allosteric signal transductions. Nat. Chem. Biol 16, 77–86 (2020). [PubMed: 31792443]
49. Cleator JH, Mehta ND, Kurtz DT & Hildebrandt JD The N54 mutant of Galphas has a conditional dominant negative phenotype which suppresses hormone-stimulated but not basal cAMP levels. FEBS Lett. 443, 205–208 (1999). [PubMed: 9989606]
50. Lee E, Taussig R & Gilman AG The G226A mutant of Gs alpha highlights the requirement for dissociation of G protein subunits. J. Biol. Chem 267, 1212–1218 (1992). [PubMed: 1730644]
51. Iiri T, Bell SM, Baranski TJ, Fujita T & Bourne HR A Gsalpha mutant designed to inhibit receptor signaling through Gs. Proc. Natl. Acad. Sci. USA 96, 499–504 (1999). [PubMed: 9892662]
52. Draper-Joyce CJ et al. Structure of the adenosine-bound human adenosine A1 receptor-Gi complex. Nature 558, 559–563 (2018). [PubMed: 29925945]
53. Danev R & Baumeister W Cryo-EM single particle analysis with the Volta phase plate. Elife 5, 439 (2016).
54. Mastronarde DN Automated electron microscope tomography using robust prediction of specimen movements. J. Struct. Biol 152, 36–51 (2005). [PubMed: 16182563]
55. Scheres SHW RELION: implementation of a Bayesian approach to cryo-EM structure determination. J. Struct. Biol 180, 519–530 (2012). [PubMed: 23000701]
56. Zivanov J et al. New tools for automated high-resolution cryo-EM structure determination in RELION-3. Elife 7, 163 (2018).
57. Zheng SQ et al. MotionCor2: anisotropic correction of beam-induced motion for improved cryo-electron microscopy. Nat. Meth 14, 331–332 (2017).
58. Zhang K Gctf: Real-time CTF determination and correction. J. Struct. Biol 193, 1–12 (2016). [PubMed: 26592709]
59. Scheres SHW & Chen S Prevention of overfitting in cryo-EM structure determination. Nat. Meth 9, 853–854 (2012).
60. Bai X-C, Rajendra E, Yang G, Shi Y & Scheres SHW Sampling the conformational space of the catalytic subunit of human γ-secretase. Elife 4, 1485 (2015).
61. Pettersen EF et al. UCSF Chimera--a visualization system for exploratory research and analysis. J. Comput. Chem 25, 1605–1612 (2004). [PubMed: 15264254]
62. Cowtan K Fitting molecular fragments into electron density. Acta Crystallogr. D Biol. Crystallogr 64, 83–89 (2008). [PubMed: 18094471]
63. Emsley P, Lohkamp B, Scott WG & Cowtan K Features and development of Coot. Acta Crystallogr. D Biol. Crystallogr 66, 486–501 (2010). [PubMed: 20383002]
64. Adams PD et al. PHENIX: a comprehensive Python-based system for macromolecular structure solution. Acta Crystallogr. D Biol. Crystallogr 66, 213–221 (2010). [PubMed: 20124702]
65. Davis IW et al. MolProbity: all-atom contacts and structure validation for proteins and nucleic acids. Nucleic Acids Res. 35, W375–83 (2007). [PubMed: 17452350]

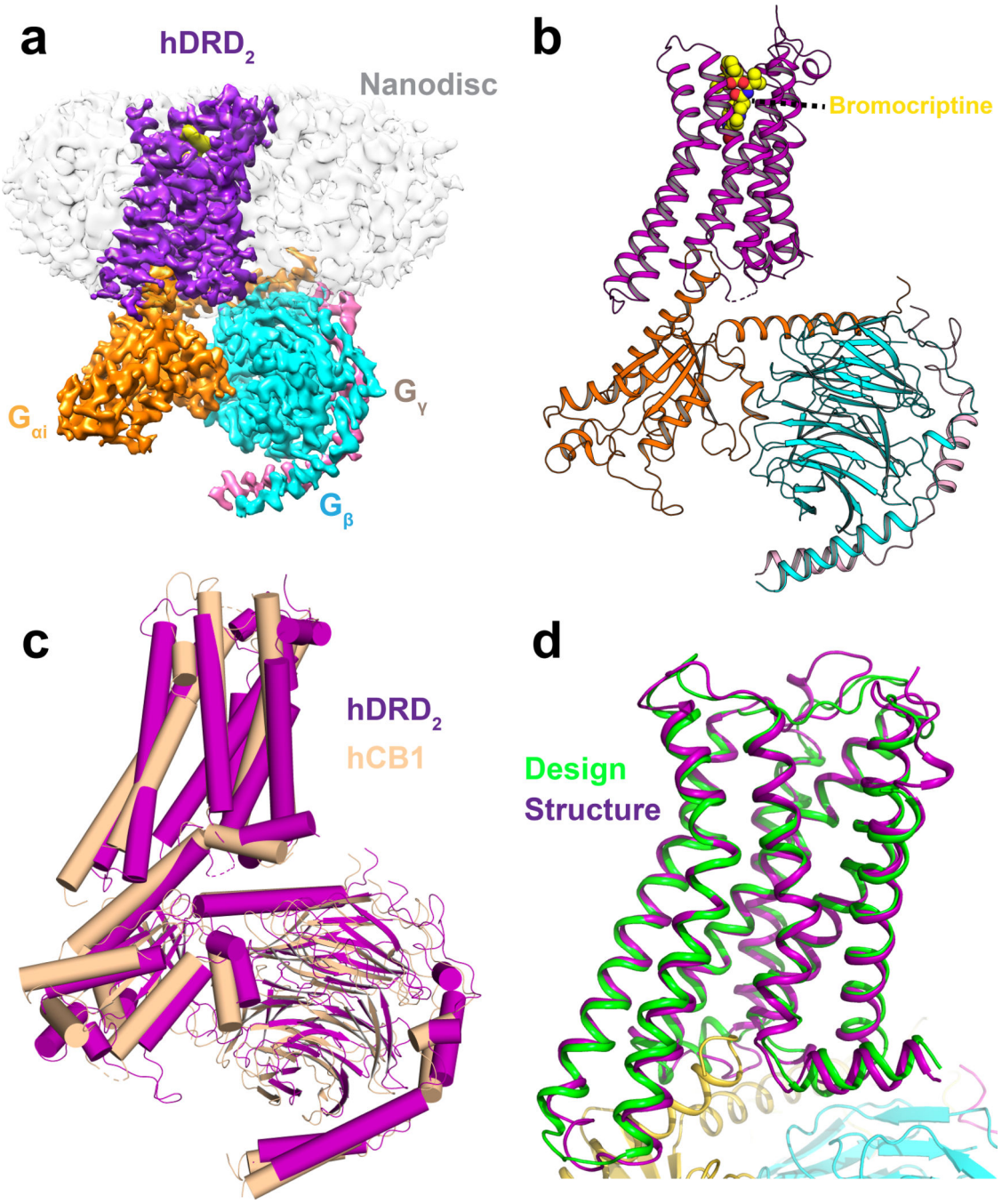

Figure 1.

Overall structure of the hDRD2^{EM}-G_i complex

(a) Cryo-EM reconstruction of the complex (density of T4L, AH domain, and scFv16 not shown). Receptor density is in purple, bromocriptine is yellow, G_α is orange, G_β is cyan, Gγ is pink.

(b) Model of complex as a cartoon, with the bromocriptine agonist as spheres with yellow carbons. scFv16, T4L, and AH domain are not shown.

(c) Superposition of the hDRD2^{EM}-G_i complex (purple) and the CB1-G_i complex (light orange).
(d) Comparison of the designed active state conformation of DRD2 (green cartoon) with the experimental structure of hDRD2^{EM} (receptor as purple cartoon). The root mean squared deviation (rmsd) for the Cα positions in the superposition is 2.1 Å.

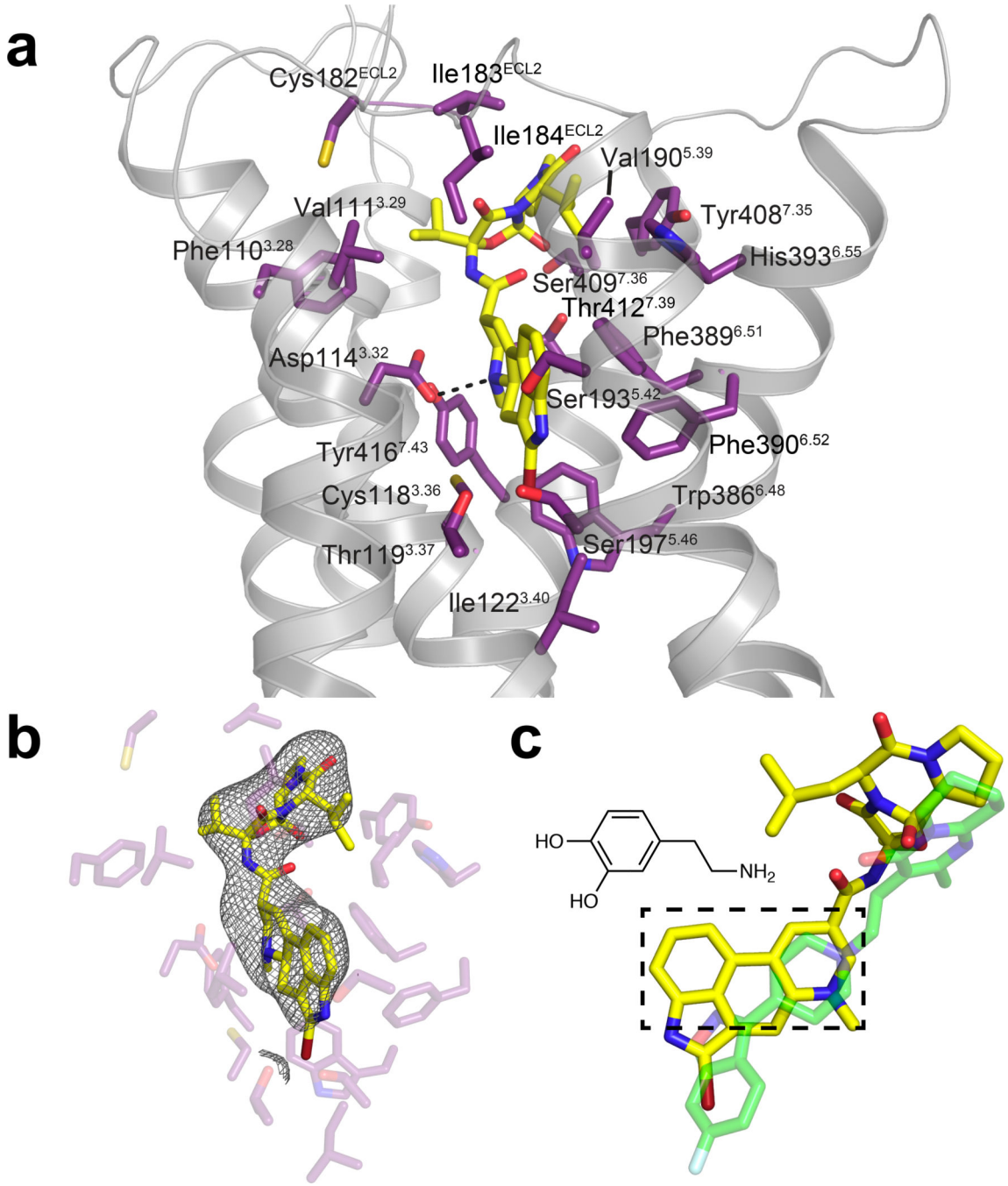

Figure 2.

Binding of bromocriptine to DRD2

(a) Contact residues (sticks with purple carbons) within 4.1 Å of bromocriptine (yellow carbons). Val115$^{3.33}$ is not shown to better illustrate the polar interaction between Asp114$^{3.32}$ and bromocriptine's amine (dotted line, 2.8 Å).

(b) Cryo-EM density surrounding the bromocriptine ligand.

(c) Overlay of bromocriptine and risperidone (transparent green sticks) when superimposing the receptor in the agonist-bound active conformation (this work) and the inverse agonist-

bound inactive conformation (PDB 6cm4). Box denotes atoms of bromocriptine analogous to dopamine (shown above as 2D structure).

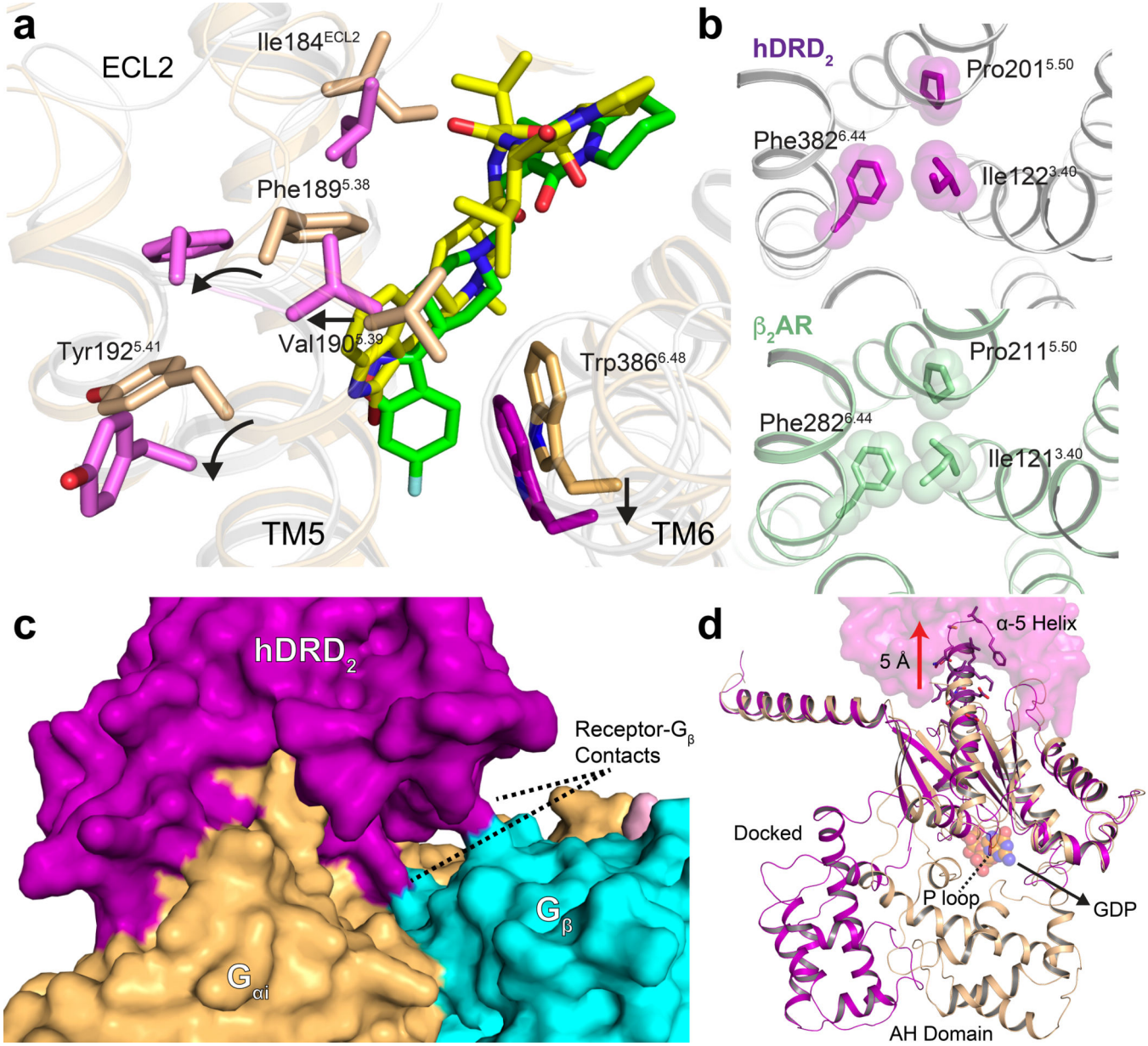

Figure 3.

Propagated changes in DRD2 activation

(a) Rotation of the upper half of TM5, comparing the active conformation (purple sticks, transparent gray cartoon) and the inactive conformation (light orange sticks and transparent cartoon, PDB 6cm4). Bromocriptine is shown as yellow sticks and risperidone is in green sticks.

(b) PIF transmission switch in the active conformation of DRD2 (upper panel, purple sticks and transparent spheres) and the active conformation of β_2AR (lower panel, PDB 3sn6, green sticks and transparent spheres).

(c) Surface representation of the receptor-G protein interface in the hDRD2^{EM}-G_i complex. Receptor is purple, Gα is orange, Gβ is cyan, and Gγ is pink.

(d) Comparison of the G_α subunit in the complex (purple cartoon) and G_α in the GDP-bound free G_i (yellow cartoon). Receptor in the complex is shown as a purple transparent surface.

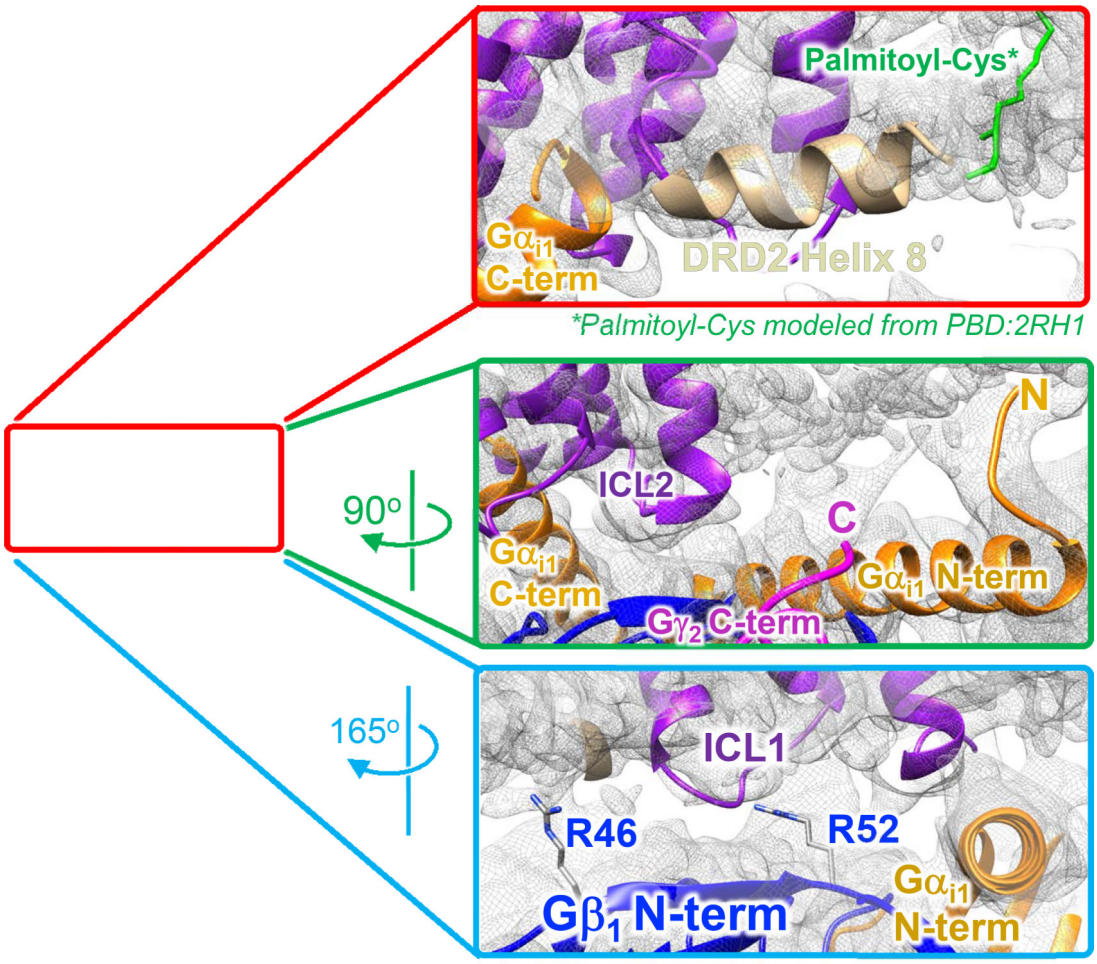

Figure 4.

Interactions of the hDRD2^{EM}-G_i complex with the rHDL/nanodisc membrane.

Cryo-EM density for the hDRD2^{EM}-G_i complex reconstituted in rHDL/nanodisc membrane highlighting densities corresponding to the receptor (purple), $G\alpha_{i1}$ (orange), $G\beta_1$ (cyan), $G\gamma_2$ (pink) and rHDL/nanodisc (gray). *(top right inset, red)* illustrates the position of helix 8 of DRD2 (tan) embedded in the phospholipid bilayer. Also rendered is the putative palmitoyl-cysteine based on the palmitoylated helix 8 of the β_2AR (PDB 2RH1). *(bottom right inset, green)* The $G\alpha_{i1}$-rHDL/nanodisc interface is highlighted by the strong EM density on the extreme amino-terminus of $G\alpha_{i1}$ (orange) and $G\gamma_2$ (magenta). Also illustrated is the $G\alpha_{i1}$ C-terminal (α5-helix) interacting with the DRD2 core. *(left inset, light blue)* Interaction of the N-terminal region of $G\beta_1$ with the phospholipid bilayer. Highlighted are residues Arg46 (R46) and Arg52 (R52).